Materials Today Bio 27 (2024) 101124

Contents lists available at ScienceDirect

Materials Today Bio

journal homepage: www.journals.elsevier.com/materials-today-bio

Cartilage decellularized matrix hydrogel loaded with protocatechualdehyde for targeted epiphycan treatment of osteoarthritis

Junchao Huang [a,1], Ziheng Bu [a,1], Wei Liu [a,1], Zheng Zhou [a], Jianhai Hu [a], Jianing Yu [a], Huajun Wang [c,**], Sudan Xu [b,***], Peng Wu [a,*]

[a] Department of Orthopedics, Shanghai Tenth People's Hospital, School of Medicine, Tongji University, Shanghai 200072, China
[b] Department of Geriatric, Shanghai General Hospital, Shanghai Jiao Tong University, School of Medicine, Shanghai 200080, China
[c] Department of Sports Medicine, The First Affiliated Hospital, Guangdong Provincial Key Laboratory of Speed Capability, The Guangzhou Key Laboratory of Precision Orthopedics and Regenerative Medicine, State Key Laboratory of Frigid Zone Cardiovascular Diseases, Jinan University, Guangzhou 510630, China

ARTICLE INFO

Keywords:
Osteoarthritis
Epiphycan
Extracellular matrix
Protocatechualdehyde
IL-17 signaling pathway
Drug delivery system

ABSTRACT

Osteoarthritis (OA) is a prevalent chronic disease, characterized by chronic inflammation and cartilage degradation. This study aims to deepen the understanding of OA's pathophysiology and to develop novel therapeutic strategies. Our study underscores the pivotal role of Epiphycan (EPYC) and the IL-17 signaling pathway in OA. EPYC, an essential extracellular matrix constituent, has been found to exhibit a positive correlation with the severity of OA. We have discovered that EPYC modulates the activation of the IL-17 signaling pathway within chondrocytes by regulating the interaction between IL-17A and its receptor, IL-17RA. This regulatory mechanism underscores the intricate interplay between the extracellular matrix and immune signaling in the pathogenesis of OA Another finding of our study is the therapeutic effectiveness of protocatechualdehyde (PAH) in OA. PAH significantly reduces chondrocyte hypertrophy and supports cartilage tissue recovery.by targets EPYC. To reduce the side effects of orally administered PAH and maintain its effective drug concentration, we have developed a decellularized matrix hydrogel loaded with PAH for intra-articular injection. This novel drug delivery system is advantageous in minimizing drug-related side effects and ensuring sustained release PAH within the joint cavity.

1. Introduction

OA, a disease associated with aging, poses a significant threat to the health of the elderly globally, particularly among those aged 65 and older [1,2]. The hallmark characteristics of OA encompass hypertrophy of the cartilage, the development of osteophytes, and hyperplasia of the synovium [3,4]. Although several causes of OA have been identified, including obesity, trauma, and genetics, its underlying mechanisms remain unclear [5,6].Currently, the research direction of OA pathogenesis is gradually shifting from solely studying chondrocytes to exploring the extracellular matrix (ECM) of chondrocytes and the local microenvironment of cartilage [7–10]. EPYC, a member of the small leucine-rich repeat proteoglycan (SLRP) family characterized by its abundance of leucine-rich repeat sequences [11]. It can interact with collagen fibers and other ECM proteins, promoting the formation of type I collagen fibers [12]. Unlike its SLRP counterparts, EPYC is predominantly expressed within cartilage, where it plays an indispensable role in both the development of cartilage and the maintenance of joint integrity [13]. It has been recently reported that EPYC is significantly upregulated in the ECM tissues of patients with OA, suggesting its potential utility as a novel biomarker for the disease's diagnosis [14]. Currently, there is a lack of further in-depth research regarding the EPYC protein.

Interleukin 17A (IL-17A) is a pro-inflammatory cytokine secreted by Th17 cells [15]. IL-17A cytokines bind to the IL-17RA/IL-17RC heterodimer, subsequently activating the IL-17 signaling pathway and triggering an immune response [16]. During the course of OA, IL-17 can influence the inflammatory response, complement production and hypoxia response [17,18]. Increasing research indicates that the ECM can regulate the binding of immune chemokines and cytokines to their corresponding receptors on the cell surface, thereby initiating changes in cellular mechanisms. Can the ECM protein EPYC regulate the binding

* Corresponding author.
** Corresponding author.
*** Corresponding author.
E-mail addresses: whj323@126.com (H. Wang), so.phie1986@163.com (S. Xu), wupeng03010814@163.com (P. Wu).
[1] These authors made equal contributions to this work.

https://doi.org/10.1016/j.mtbio.2024.101124
Received 16 February 2024; Received in revised form 16 May 2024; Accepted 12 June 2024
Available online 15 June 2024

Abbreviations and acronyms:

ADAMTS-4	A Disintegrin And Metalloproteinase with Thrombospondin Motifs 4
co-IP	co-immunoprecipitation
DECM	decellularized matrix
DMM	Damaging the medial meniscus
DSPG3	Dermatan sulfate proteoglycan 3
EPYC	Epiphycan
ECM	Extracellular matrix
EDTA	ethylenediaminetetraacetic acid
GO	Gene Ontology
GAPDH	Glyceraldehyde-3-phosphate dehydrogenase
H&E	Hematoxylin and Eosin
IL-17	Interleukin 17
KEGG	Kyoto Encyclopedia of Genes and Genomes
MTP	Medial tibia plateau
MFC	Medial femoral condyle
MCP-1	Monocyte Chemoattractant Protein-1
OA	Osteoarthritis
OARSI	Osteoarthritis Research Society International
PGs	Proteoglycans
PFA	paraformaldehyde
PGE2	Prostaglandin E2
PG-Lb	proteoglycan-Lb
PAH	Protocatechualdehyde
PVDF	Polyvinylidene fluoride
SOFG	Safranin O/Fast Green
SEM	Scanning electron microscope
SLRP	Small leucine-rich repeat proteoglycan
SDS-PAGE	SDS-polyacrylamide gel electrophoresis

of inflammatory factors like IL-17A to receptors on the surface of chondrocytes? This is one of our primary research focuses.

Commonly used drug treatments in clinical practice, such as non-steroidal anti-inflammatory drugs, have side effects, such as gastrointestinal discomfort [19,20]. Therefore, finding a drug with fewer side effects to reverse the progression of OA is crucial. PAH, a natural phenolic compound found in the traditional Chinese herb Salvia miltiorrhiza, is known for its anti-inflammatory and antioxidant, with minimal toxic side effects [21–24]. Recent studies have revealed that PAH can protect human dermal fibroblasts from photoaging by inhibiting the expression of matrix metalloproteinases and pro-inflammatory factors [25], Whether PAH can exert its anti-inflammatory effects in OA remains unknown, as there are currently no studies on its mechanism of action in this context.

To achieve prolonged drug release of PAH within the organism and enhance its targeting towards EPYC, a bioactive scaffold with good biocompatibility, mechanical properties, and biodegradability is essential. Cartilage decellularized matrix (DECM) hydrogel has the advantage of reduced immunogenicity while retaining the components, structure, and function of the ECM [26,27]. Given the presence of aldehyde and hydroxyl groups in PAH, it is capable of engaging in a Schiff base reaction with amines in an alkaline setting, suggesting that PAH can chemically bond with the DECM hydrogel. This interaction is anticipated to augment the hydrogel's mechanical and biological attributes. Furthermore, as the DECM hydrogel degrades, it can facilitate a controlled release of PAH.As EPYC is a component of the ECM of cartilage, using cartilage DECM hydrogel loaded with PAH will provide more opportunities for PAH to interact with EPYC, thereby enhancing its therapeutic efficacy of OA. In this experiment, we successfully prepared the PAH@DECM hydrogel, achieving the slow release of PAH. With the degradation of DECM, the released PAH is gradually utilized by chondrocytes, playing roles in anti-inflammation and promoting chondrocyte migration and proliferation.

In this study, we report for the first time that in OA, the upregulated expression of EPYC enhances the binding of the inflammatory chemokine IL-17A to its chondrocyte surface receptor IL-17RA, further activating the IL-17 signaling pathway and exacerbating the progression of OA. We have discovered for the first time that PAH has a therapeutic effect on OA and can act on EPYC to downregulate its expression, reversing the pro-OA effects of EPYC. Leveraging these insights, and aiming to mitigate the first-pass effect and minimize PAH's side effects, we have engineered a composite material consisting of PAH and DECM hydrogel. This innovative combination is anticipated to augment the therapeutic efficacy of PAH in the treatment of OA. These findings are of significant importance for a deeper understanding of the pathogenesis of OA and the development of new treatment methods (Graphical Abstract).

2. RESULTs

2.1. EPYC can regulate the progression of OA

Fig. 1A serves as a summary diagram for the content of this section. To identify genes with differential expression in OA, we sourced datasets GSE55235 and GSE55457 from the GEO database, encompassing sequencing data from both 20 healthy and 20 OA-affected joint tissues. After analyzing the GSE data, we created volcano plots (Fig. 1B) and heatmaps (Supplementary S1A). Relative to the healthy control group, there was a marked decrease in the expression levels of molecules like SIK1, APOLD1, and GRB10 within the OA group, whereas an increase was observed for CX3CR1, EPYC, SCRG1, among others (Fig. 1C). Current research on OA is gradually expanding from focusing solely on chondrocytes to encompassing the microenvironment in which chondrocytes exist. The ECM and collagen fibers form the scaffold of cartilage tissue and constitute the primary living environment for chondrocytes, while also serving as substrates for the ADAMs family of proteases and the MMPs family of proteases. Consequently, EPYC, one of the differentially expressed genes highlighted above, has garnered our interest. EPYC is a proteoglycan from the type III SLRPs family and is a component of the ECM. It interacts with collagen fibers and the ECM, facilitating the synthesis of type I collagen fibers, and is crucial for cartilage development and the preservation of joint integrity [13]. Recently, it has been reported to be associated with the development of OA and may serve as a novel biomarker for diagnosing OA [14]. In light of these findings, we intend to further explore the regulatory mechanisms of EPYC in the etiology and progression of OA Further mining of the GSE datasets with a focus on EPYC revealed significant differences in the expression levels of EPYC between healthy individuals and those with OA (Fig. 1D). The constructed ROC curve also suggests that EPYC possesses high diagnostic sensitivity for OA (Fig. S1B).

Next, to validate the differential expression of EPYC in the GSE dataset, we established an in vivo OA DMM animal model. Regularly harvested rat cartilage sections demonstrated a significant upregulation of EPYC expression in cartilage tissue following DMM surgery, as evidenced by immunohistochemistry (Fig. 1E). Hematoxylin and Eosin (H&E) and Safranin O-fast green (SOFG) staining revealed that, compared to sham rats, cartilage damage, significant loss of collagen fibers, and reduced joint space occurred post-DMM surgery, suggesting that increased EPYC expression is associated with cartilage degeneration and OA progression (Fig. 1FG). The OARSI scores for the medial tibia plateau (MTP) and medial femoral condyle (MFC) (Fig. S1C), as well as the total OARSI score, were calculated, showing a significant increase in

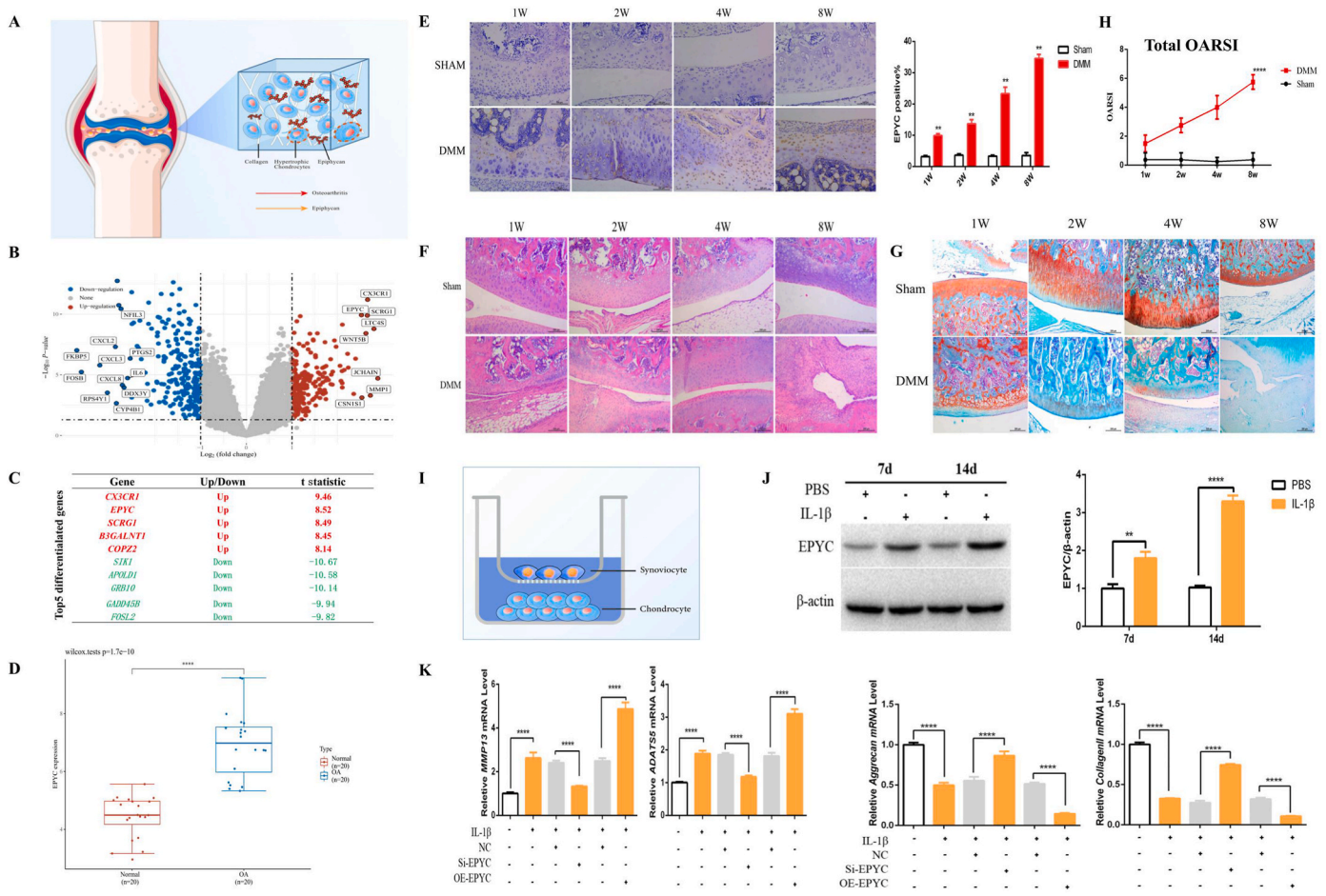

Fig. 1. **(A)** The expression level of EPYC is elevated in OA, and it plays a regulatory role in determining the severity of OA. **(B)** Volcano plots obtained through the analysis of datasets GSE55235 and GSE55457. **(C)** The top 5 upregulated and downregulated genes with the most significant differential expression in the datasets. **(D)** The expression difference of EPYC between the Normal group and the OA group in the dataset.wilcox.tests p = $1.7e^{-10}$.**(E)** Immunohistochemical staining results of EPYC at different weeks in the Sham and DMM groups, along with corresponding bar charts. Scale bar, 100 μm. All data are presented as mean ± SD; N = 3; **P < 0.01. **(F)** H&E and **(G)**SOFG staining results in the Sham and DMM groups at different weeks.Scale bar, 200 μm. N = 3. **(H)** OARSI score in the Sham and DMM groups. All data are presented as mean ± SD; N = 6, ****P < 0.0001. **(I)** Schematic illustration for synoviocyte-chondrocyte co-culture model. **(J)** Observation of EPYC expression level changes at 7 and 14 days post IL-1β stimulation in the co-culture model using in vitro Western Blot analysis. along with corresponding bar charts. All data are presented as mean ± SD; **P < 0.01, ****P < 0.0001. **(K)** Using RT-PCR to observe changes in the transcription levels of MMP13, ADATS5, Aggrecan, and Collagen II following the overexpression and knockdown of EPYC. All data are presented as mean ± SD; N = 3, ****P < 0.0001.

OARSI scores in rats post-DMM surgery (Fig. 1H). We also built an in vitro synovial cell-chondrocyte co-culture model. Synovial cells were cultured in the upper chamber of a transwell co-culture system, while chondrocytes were cultured in the lower chamber, both treated with IL-1β (Fig. 1I). synoviocytes secrete a range of immune chemokines and inflammatory factors, including IL-17, IL-6, TNF, etc., playing a significant role in regulating the joint microenvironment and stimulating catabolic pathways in chondrocytes [28]. Western blot in vitro results from cell experiments were consistent with the immunohistochemistry results from animal experiments, showing increased expression of EPYC at both 7D and 14D time points in the synoviocyte-chondrocyte co-culture model (Fig. 1J). To examine EPYC's regulatory influence in OA, we engineered plasmids for both overexpression and knockdown of EPYC, subsequently assessing their efficacy (Fig. S1D). PCR results after transfecting the synoviocyte-chondrocyte co-culture model with plasmids indicated that overexpression of EPYC further inhibited the transcription levels of the proteoglycan Aggrecan and collagen fiber Col2, while increasing the transcription levels of the proteases ADATS5 and MMP13. Knockdown of EPYC could reverse the hypertrophy of chondrocytes stimulated by IL-1β (Fig. 1K). These results suggest that EPYC expression levels rise in OA, and it can regulate the severity of OA.

2.2. EPYC can regulate the expression of IL-17A

Fig. 2A provides a summary diagram for the content of this section. The differentially expressed genes derived from the GSE dataset underwent Gene Ontology (GO) and Kyoto Encyclopedia of Genes and Genomes (KEGG) enrichment analysis. GO enrichment analysis revealed that in OA patients, as compared to healthy individuals, there is abnormal activation of leukocytes, dysregulated activity of chemokines, disrupted chemokine-mediated signaling pathways, and disturbance in chemokine homeostasis. Chemokines are intimately connected to inflammation, which is, in turn, tightly coupled with alterations in the inflammatory microenvironment. This guides the onset and progression of a range of diseases, including OA, heterotopic ossification, and osteosarcoma [29,30]. (Fig. 2B). KEGG results indicated that most differentially expressed genes are related to the IL-17 signaling pathway (Fig. 2C). The IL-17 signaling pathway has been repeatedly reported in relation to OA. The IL-17 family consists of six cytokines (IL-17A to F), with IL-17A being the most extensively studied and considered the most influential [15,17,31,32]. Studies have shown that the levels of IL-17A in the serum and synovial fluid of OA patients are higher than those in healthy individuals and are positively correlated with measures of pain, functionality, and disease severity [18,33]. When comparing

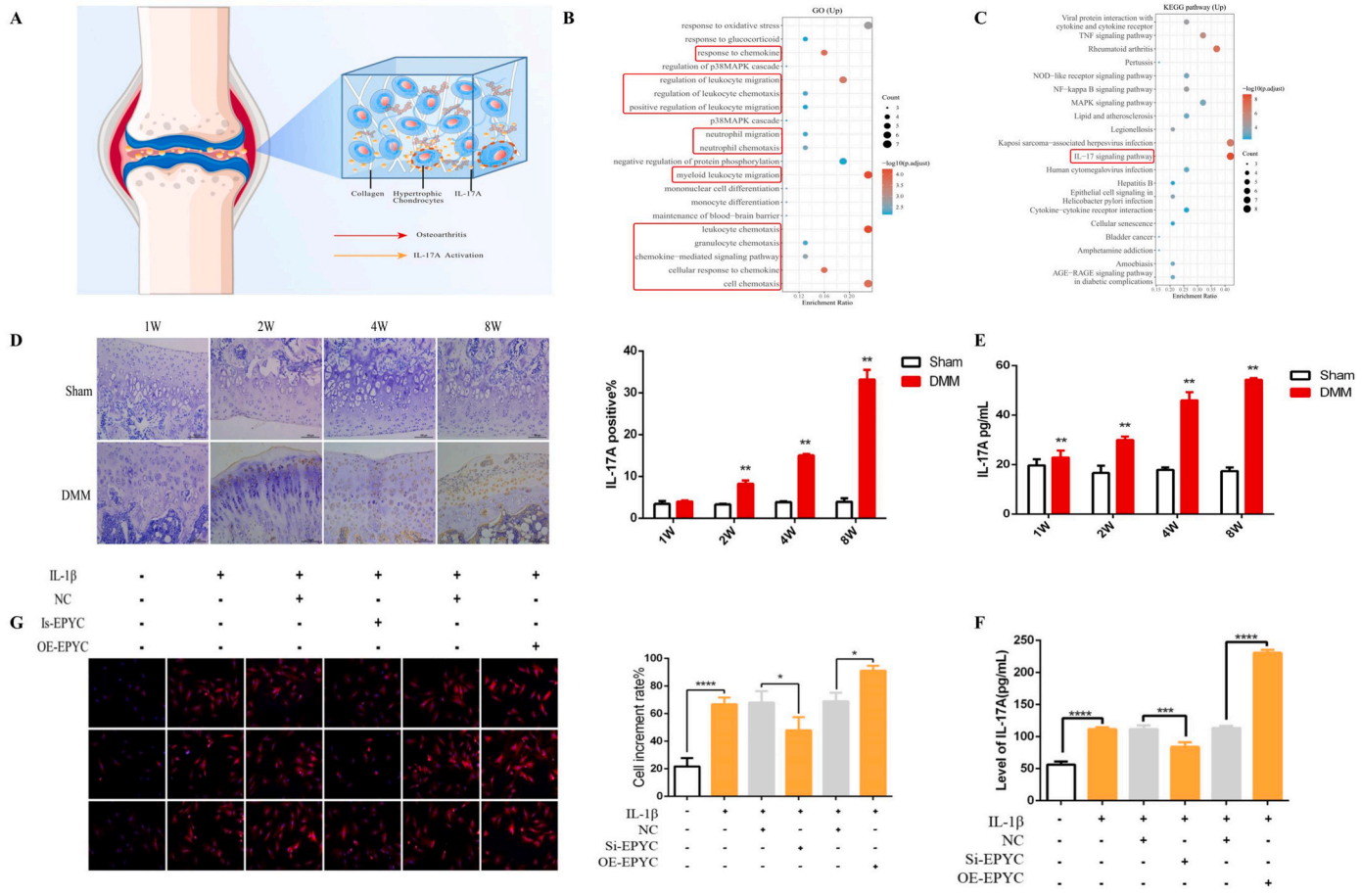

Fig. 2. **(A)** In OA, IL-17A exhibited increased expression levels and was regulated by EPYC. **(B)** GO analysis of datasets GSE55235 and GSE55457. **(C)** KEGG analysis of datasets GSE55235 and GSE55457. **(D)** Immunohistochemical staining results of IL-17A at different weeks in the Sham and DMM groups, along with corresponding bar charts. Scale bar, 100 μm. All data are presented as mean ± SD; N = 3; **P < 0.01. **(E)** ELISA experiments were conducted on tissue samples from Sham and DMM groups at various weeks to observe the concentration of IL-17A. All data are presented as mean ± SD; N = 3; **P < 0.01. **(G)** Immunofluorescence assays were conducted in the co-culture model to investigate the alterations in IL-17A localization following EPYC knockdown and overexpression, along with corresponding bar charts. Scale bar, 100 μm. All data are presented as mean ± SD; N = 3; *P < 0.05. ****P < 0.0001. **(F)** In the co-culture in vitro model, ELISA experiments were conducted to observe changes in IL-17A concentration following the knockdown and overexpression of EPYC. All data are presented as mean ± SD; N = 3; ***P < 0.001. ****P < 0.0001.

inflammatory and non-inflammatory synovium in OA patients, it was found that IL-17A concentration is increased in inflammatory OA tissues, associated with the release of IL-6, IL-23, and TGF-β1 [34]. To validate the role of IL-17A in OA, we first conducted animal validation experiments. Immunohistochemistry (Fig. 2D) and ELISA (Fig. 2E) results demonstrated significantly higher IL-17A expression levels in the knee joints of rats subjected to DMM surgery than in those of the control group. The IL-17A cytokine, by binding to the IL-17RA/IL-17RC heterodimer complex, activates downstream signaling pathways, leading to an immune response [35]. Research indicates that the ECM regulates cellular activity states by either blocking or promoting the binding of cytokines to cell surface receptors. As established in the previous section, we have confirmed the upregulation of the ECM component EPYC in OA. Therefore, we considered whether EPYC could regulate the IL-17 signaling pathway by modulating the binding of IL-17A to its receptor IL-17RA. Immunofluorescence results from the co-culture model showed that after IL-1β treatment, co-localization of IL-17A with chondrocytes increased, suggesting accumulation of IL-17A at chondrocyte surface receptors. Overexpression of EPYC could enhance this trend, while knocking down EPYC could reverse it (Fig. 2G). ELISA results from the synoviocyte-chondrocyte co-culture model suggested that overexpression of EPYC can enhance the chemotactic properties of IL-17A secreted by synoviocytes, accumulating in the underlying chondrocytes (Fig. 2F). These results suggest that during the course of OA, the secretion of the chemokine IL-17A is dysregulated, the IL-17 signaling pathway in chondrocytes is activated, and EPYC plays a regulatory role in this process.

2.3. PAH can alleviate the symptoms of OA

Fig. 3A presents a summary diagram of the content for this section. Having previously established the regulatory effects of EPYC on OA and IL-17A, we now proceed to investigate novel therapeutic strategies that target EPYC. PAH, an active component of the natural product Salvia miltiorrhiza, possesses various pharmacological activities including anti-inflammatory and antioxidant properties (Fig. 3B). PAH has been reported to have excellent anti-inflammatory and antioxidant properties. It can promote diabetic wound healing in an inflammatory environment by modulating macrophage polarization and has been proven to protect endothelial cells from TNF-α-induced damage by inhibiting the expression of ICAM-1 and VCAM-1, as well as by stimulating macrophage RAW264.7 to scavenge free radicals [21], thereby exerting its anti-inflammatory and antioxidant effects. As is widely known, inflammation plays a crucial role in OA. The potential of PAH to manifest anti-inflammatory effects within the context of OA has yet to be explored, given the current absence of studies regarding its therapeutic application in OA. Molecular docking experiments were conducted to assess the interaction between PAH and EPYC. The docking results show

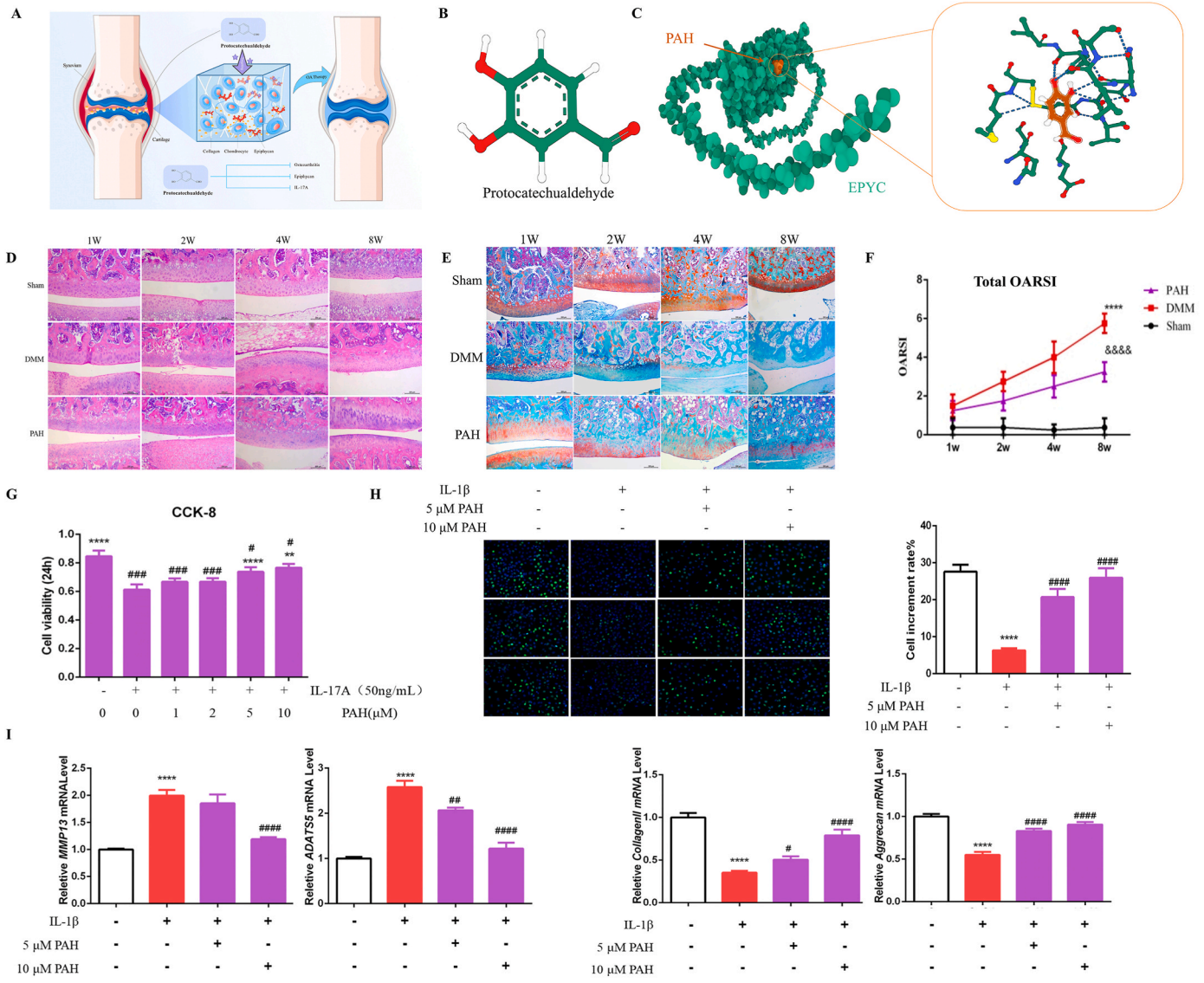

Fig. 3. **(A)** PAH is capable of treating OA. **(B)** The molecular structure of protocatechualdehyde comprises a benzene ring with two hydroxyl groups (-OH) attached to adjacent carbon atoms (positions 3 and 4), and an aldehyde group (-CHO) attached to the benzene ring at position 1. This arrangement categorizes PAH as a dihydroxybenzaldehyde. The hydroxyl groups and aldehyde group are responsible for its chemical properties and biological activities. **(C)** Schematic diagram of the molecular docking between PAH and EPYC, and the Illustration of the interaction sites between PAH and EPYC. **(D)** H&E staining results in the Sham, DMM and PAH groups at different weeks.Scale bar, 200 μm. N = 3. **(E)** SOFG staining results in the Sham, DMM and PAH groups at different weeks.Scale bar, 200 μm. N = 3. **(F)** total OARSI score, in the Sham, DMM and PAH groups. All data are presented as mean ± SD; N = 6, ****P < 0.0001, compared with Sham group. &&&& < 0.0001, compared with DMM group. **(G)** After administering IL-17A (50 ng/mL) and various concentrations of PAH to chondrocytes, changes in chondrocyte proliferation levels were observed using the CCK8 assay. All data are presented as mean ± SD; N = 6, **P < 0.01, ****P < 0.0001, compared with IL-17A (+) PAH (−) group. #< 0.05, ### < 0.001, compared with IL-17A (−) PAH (−) group. **(H)** Results of Edu staining and corresponding bar graphs for in vitro co-cultured cells treated with different concentrations of PAH. All data are presented as mean ± SD; N = 3, ****P < 0.0001, compared with IL-1β (−) PAH (−) group. #### < 0.0001, compared with IL-1β (+) PAH (−) group. **(I)** Using RT-PCR to observe changes in the transcription levels of MMP13, ADATS5, Aggrecan, and Collagen II following the administration of\ PAH. All data are presented as mean ± SD; N = 3, ****P < 0.0001, compared with IL-1β (−) PAH (−) group. # < 0.05, ## < 0.01, #### < 0.0001, compared with IL-1β (+) PAH (−) group.

that PAH and EPYC molecules have multiple potential hydrogen bond binding sites (Fig. 3C) and good binding affinity (Supplementary materials 1). This suggests that PAH may target EPYC and have potential therapeutic effects on OA. H&E (Fig. 3D) and SOFG (Fig. 3E) staining demonstrated significant inflammatory cell infiltration in the DMM group during the first week, which was less pronounced in the PAH group. By the second week, the DMM group exhibited joint cartilage damage characterized by surface fissures and minor cartilage loss, while the PAH group showed comparable but milder damage. At four weeks, the DMM group presented with more profound cartilage damage, penetrating approximately halfway into the joint surface, whereas the PAH group demonstrated cartilage loss with some surface erosion. By eight weeks, the DMM group displayed a complete absence of a normal cartilage layer, contrasting with the PAH group, which showed cartilage surface erosion but without deep penetration.

After the DMM surgery in rats, the OARSI score increased, which was reversed following the administration of PAH (Fig. S2A, Fig. 3F). Thereafter, the therapeutic effects and underlying mechanisms of PAH on osteoarthritis were further substantiated through cellular assays. Initially, the optimal concentration of PAH for cellular experiments was ascertained using the CCK8 assay. The findings at 24 and 48 h suggested minimal effects on chondrocyte proliferation at concentrations below

10 μM, prompting the selection of 5 μM and 10 μM for subsequent experiments (Fig. 3G). SOFG of chondrocytes showed that administration of PAH significantly reversed the loss of cartilage matrix in chondrocyte in a concentration-dependent manner (Fig. S2B). Edu staining results indicated that PAH administration inhibited apoptosis in chondrocytes and increased the number of highly proliferative cells (Fig. 3H). PCR assay results demonstrated that PAH administration suppressed the transcription of hypertrophic markers, including ADAMTS5 and MMP13, in chondrocytes while upregulating the transcription of ECM components such as COL2 and Aggrecan (Fig. 3I). During OA onset, joints are infiltrated by inflammatory factors, limiting proliferation and increasing apoptosis of chondrocytes, and accelerating the loss of collagen fibers and proteoglycans in the ECM. Our experimental results suggest that PAH can similarly exert its anti-inflammatory effects in OA, protecting chondrocytes and the ECM.

2.4. PAH can regulate the expression of EPYC and IL-17A

In the previous section, we confirmed the therapeutic effect of PAH on OA; hence, we plan to further investigate whether PAH exerts its therapeutic action on OA by acting on EPYC and IL-17A. Immunohistochemical analysis of animal tissue sections indicates that PAH administration significantly diminishes the expression levels of EPYC (Fig. 4A) and IL-17A (Fig. 4B). In the DMM animal model and synoviocyte-chondrocyte co-culture model, Western Blots (Fig. 4C–F) and ELISA experiments (Fig. 4D and E) were performed. These assays, aligning with the immunohistochemical findings, demonstrated that PAH downregulates the expression levels of EPYC and IL-17A. In vitro IL-17A immunofluorescence experiments also showed that PAH decreases the co-localization of IL-17A with chondrocytes in a concentration-dependent manner (Fig. 4G). Collectively, these findings imply that the therapeutic effectiveness of PAH in the treatment of OA may be realized through its modulation of EPYC and IL-17A.

2.5. EPYC regulated the binding of IL-17A to IL-17RA in chondrocytes

Fig. 5A is the summary diagram of this section's content. In the preceding section, we established that EPYC and IL-17A contribute to the pathogenesis of OA, with EPYC modulating IL-17A. This prompted us to investigate whether EPYC's pro-OA effect is mediated through the regulation of IL-17A. To verify this, we conducted Rescue experiments. PCR findings (Fig. 5B) indicated that administering IL-1β to the synoviocyte-chondrocyte co-culture elevates the transcription of hypertrophic markers like ADATS5 and MMP13 in chondrocytes. This elevation is negated by EPYC knockdown, but further administration of IL-17A (50 ng/mL) reverses this negation. Similarly, EPYC knockdown reverses the IL-1β-induced downregulation of cartilage matrix components, including COL2 and Aggrecan. However, adding IL-17A subsequently leads to a decrease in their transcription levels again. SOFG and Edu staining results align with PCR findings. Administering IL-17A alone promotes cartilage matrix loss; knocking down EPYC alone reverses this phenotype of cartilage matrix loss; concurrently administering IL-17A

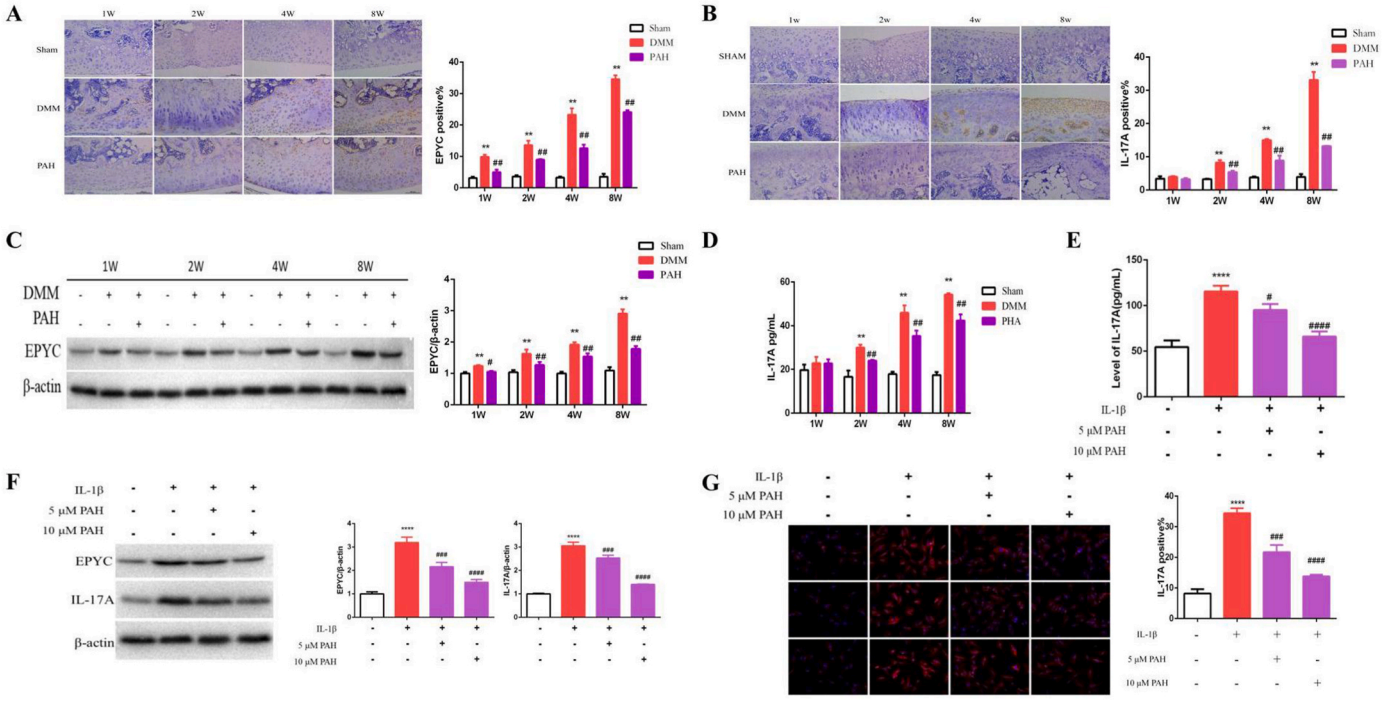

Fig. 4. PAH exerts regulatory effects on EPYC and IL-17A. **(A)** Results of immunohistochemical experiments for EPYC on pathological sections from DMM rat models treated with PAH, along with corresponding bar graphs. Scale bar, 100 μm. All data are presented as mean ± SD; N = 3; **P < 0.01. compared with Sham group. ##P < 0.01. compared with DMM group. **(B)** Results of immunohistochemical experiments for IL-17A on pathological sections from DMM rat models treated with PAH, along with corresponding bar graphs. Scale bar, 100 μm. All data are presented as mean ± SD; N = 3; **P < 0.01. compared with Sham group. ##P < 0.01. compared with DMM group. **(C)** Results of Western Blot experiments and corresponding bar graphs for tissue samples harvested at different weeks from rat models treated with PAH. All data are presented as mean ± SD; **P < 0.01. compared with Sham group. #P < 0.05, ##P < 0.01. compared with DMM group. **(D)** ELISA experiments were conducted on tissue samples from Sham, DMM and PAH groups at various weeks to observe the concentration of IL-17A. All data are presented as mean ± SD; N = 3; **P < 0.01. compared with Sham group. ##P < 0.01. compared with DMM group. **(E)** Conducting ELISA experiments in the in vitro co-culture model to observe the concentration results of IL-17A before and after administering PAH. All data are presented as mean ± SD; N = 3; **P < 0.01. compared with Sham group. #P < 0.05, ##P < 0.01. compared with DMM group. **(F)** Conducting Western Blot experiments in the in vitro co-culture model to observe the changes in expression levels of EPYC and IL-17A before and after administering PAH, along with corresponding bar graphs. ****P < 0.0001. compared with IL-1β (−) PAH (−) group. ###P < 0.001, ####P < 0.0001. compared with IL-1β (+) PAH (−) group. **(G)** Performing immunofluorescence experiments in the in vitro co-culture model to observe changes in the co-localization of IL-17A with chondrocytes before and after administering PAH, along with corresponding bar graphs. Scale bar, 100 μm. N = 3, ****P < 0.0001. compared with IL-1β (−) PAH (−) group. ###P < 0.001, ####P < 0.0001. compared with IL-1β (+) PAH (−) group.

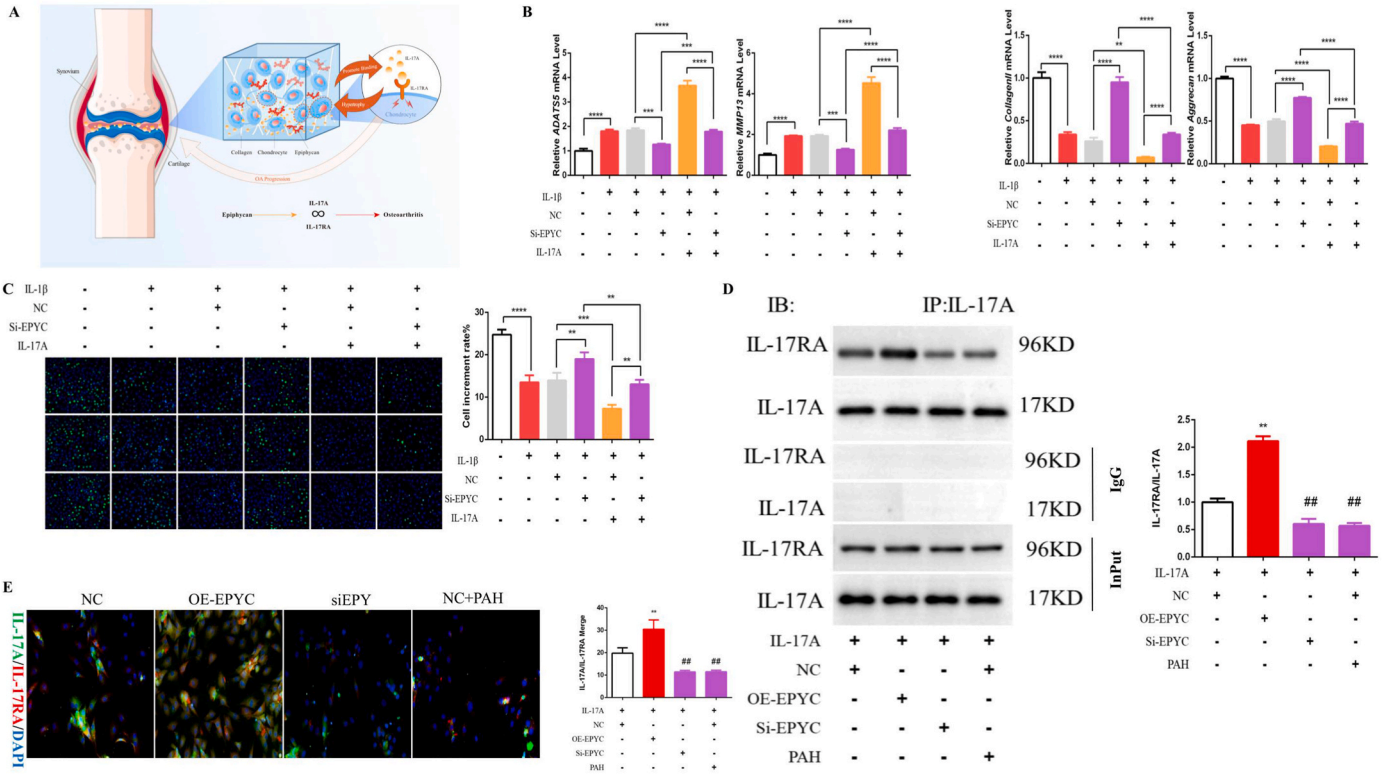

Fig. 5. **(A)**The control of EPYC over the severity of OA is contingent upon its influence on the functions of IL-17A. **(B)** Using RT-PCR to observe changes in the transcription levels of MMP13, ADATS5, Aggrecan, and Collagen II in vitro chondrocytes following the knockdown of EPYC and simultaneous administration of IL-17A (50 ng/mL). All data are presented as mean ± SD; N = 3, ***P < 0.001. ****P < 0.0001. **(C)** Observing changes in chondrocyte proliferation levels in vitro chondrocytes using Edu staining following the knockdown of EPYC and simultaneous administration of IL-17A (50 ng/mL), along with corresponding bar charts. Scale bar, 100 μm. N = 3, **P < 0.01, ***P < 0.001, ****P < 0.0001. **(D)** Conducting co-immunoprecipitation (co-IP) experiments to observe changes in the binding levels of IL-17A to IL-17RA in chondrocytes under IL-17A stimulation in vitro, following either overexpression or knockdown of EPYC, or administration of PAH. **P < 0.01. compared with OE-EPYC (−) Si-EPYC (−) PAH (−) group. ##P < 0.01. compared with OE-EPYC (+) Si-EPYC (−) PAH (−) group. **(E)** Conducting immunofluorescence experiments to observe the changes in the co-localization levels of IL-17A with chondrocytes under IL-17A stimulation in vitro, following either overexpression or knockdown of EPYC, or administration of PAH. Scale bar, 100 μm. N = 3, **P < 0.01. compared with OE-EPYC (−) Si-EPYC (−) PAH (−) group. ##P < 0.01. compared with OE-EPYC (+) Si-EPYC (−) PAH (−) group.

with EPYC knockdown reverses the effect of EPYC knockdown alone, exacerbating chondrocyte apoptosis and reducing proliferation (Fig. S3A, Fig. 5C). To further ascertain whether EPYC can modulate the binding of IL-17A to its receptor IL-17RA, we performed experiments to assess the interaction between IL-17A and IL-17RA. Results show that administering IL-1β can promote the binding of IL-17A to its receptor IL-17RA, while overexpressing EPYC further enhances this binding. Knocking down EPYC has the opposite effect (Fig. 5D). Dual immunofluorescence staining for IL-17A and IL-17RA reveals that EPYC overexpression increases the co-localization of IL-17A with its receptor IL-17RA. Conversely, knocking down EPYC or administering PAH reduces the overlap of IL-17A/IL-17RA fluorescence staining (Fig. 5E).The results suggest that the pro-OA effect of EPYC depends on mediating the binding of IL-17A to its receptor IL-17RA.

2.6. The therapeutic effect of PAH on OA is dependent on its regulatory mechanism on EPYC

Fig. 6A is the summary diagram of this section's content. In our previous studies, we demonstrated that EPYC exacerbates OA by modulating the interaction between IL-17A and IL-17RA. Additionally, PAH has been validated as a therapeutic agent for OA. Based on this, we speculate that PAH may indirectly affect IL-17A by targeting EPYC, thereby offering therapeutic benefits for OA. To validate this hypothesis, we conducted a series of experiments. In our co-culture system, we found that PAH significantly reversed the increase in transcription levels of hypertrophic markers like ADATS5 and MMP13 induced by IL-1β. Nonetheless, the overexpression of EPYC alone exacerbated the hypertrophic tendency of chondrocytes. Encouragingly, simultaneous administration of PAH could reverse the adverse effects brought by overexpression of EPYC. The results for cartilage ECM markers such as COL2 and Aggrecan were opposite (Fig. 6B). SOFG and Edu staining indicated that overexpression of EPYC exacerbated the loss of cartilage matrix, but this was mitigated by co-administering PAH, reducing collagen loss and other consequences of EPYC overexpression (Fig. S4A). In the in vitro ELISA experiments, we noted a significant reduction in IL-17A accumulation in chondrocytes after simultaneous administering PAH compared to the overexpression of EPYC alone (Fig. 6C). Furthermore, administering PAH alongside EPYC overexpression could reverse the effects of EPYC overexpression alone, thereby enhancing chondrocyte proliferation and reducing apoptosis (Fig. 6D). Immunofluorescence assessment of IL-17A showed that IL-1β administration resulted in IL-17A accumulation on chondrocyte surfaces, a phenomenon that was further amplified by the overexpression of EPYC. Notably, concurrent administration of PAH could reverse the IL-17A accumulation effect caused by EPYC overexpression (Fig. 6E). co-IP results show that administering PAH has an effect similar to knocking down EPYC, significantly reducing the binding of IL-17A to IL-17RA (Fig. 5D) . Synthesizing these findings, we conclude that the therapeutic efficacy of PAH in treating OA is attributable to its direct modulation of EPYC and its indirect regulation of IL-17A. This discovery provides an important theoretical basis for developing new OA treatment strategies.

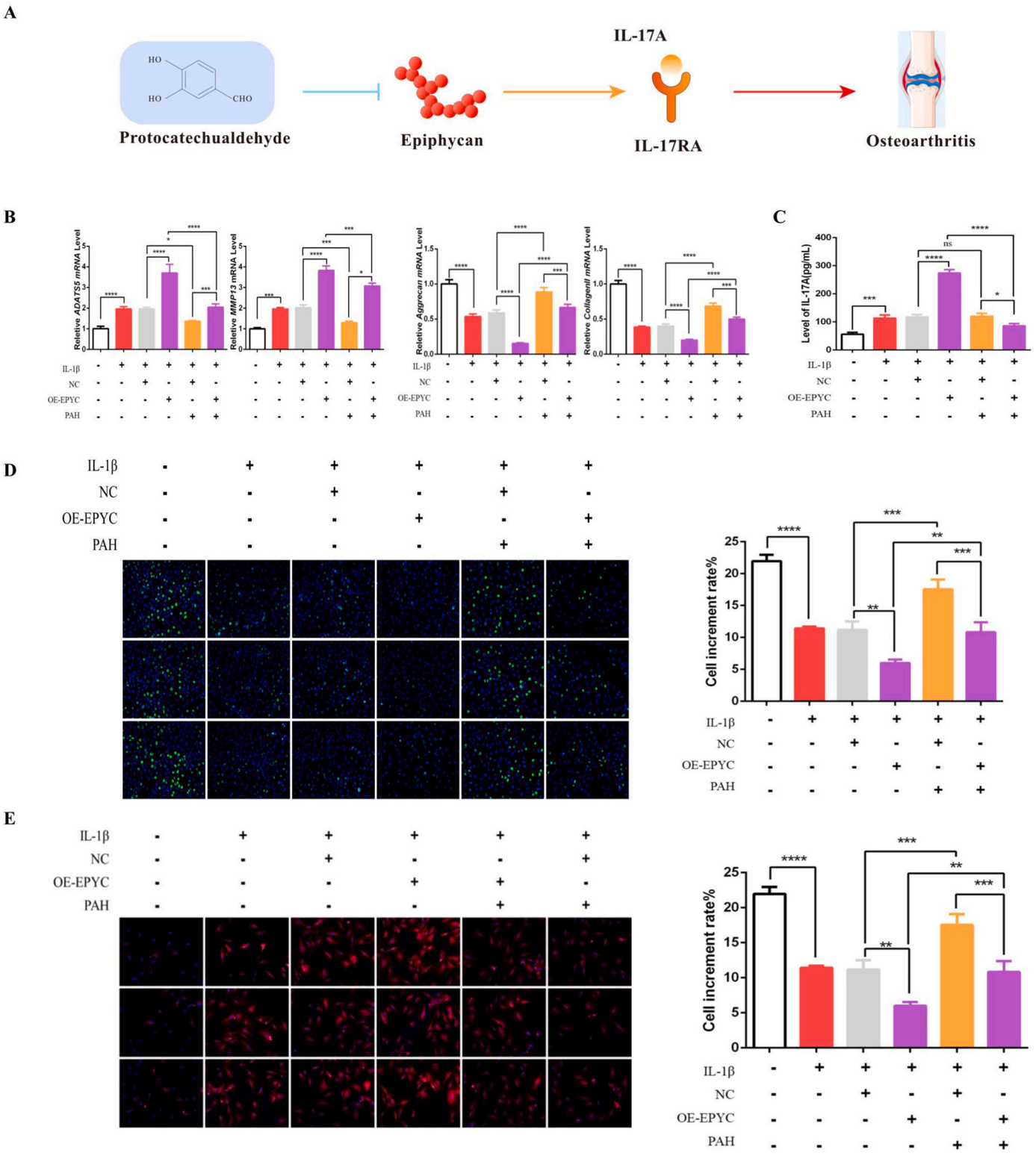

Fig. 6. (A) The therapeutic efficacy of PAH in treating OA is dependent on EPYC. **(B)** Using RT-PCR to observe changes in the transcription levels of MMP13, ADATS5, Aggrecan, and Collagen II in vitro chondrocytes following the overexpression of EPYC and simultaneous administration of PAH (10 μM). All data are presented as mean ± SD; N = 3, *P < 0.05, ***P < 0.001, ****P < 0.0001.**(C)** Conducting ELISA experiments to observe changes in the concentration levels of IL-17A in co-culture model under IL-1β stimulation in vitro, following the overexpression of EPYC and simultaneous administration of PAH. All data are presented as mean ± SD; N = 3, *P < 0.05, ***P < 0.001, ****P < 0.0001. **(D)** Observing changes in chondrocyte proliferation levels in vitro chondrocytes using Edu staining following the overexpression of EPYC and simultaneous administration of PAH (10 μM), along with corresponding bar charts. Scale bar, 100 μm. N = 3, **P < 0.01, ***P < 0.001, ****P < 0.0001. **(E)** Conducting immunofluorescence experiments to observe the changes in the co-localization levels of IL-17A with co-culture model under IL-1β stimulation in vitro, following overexpression of EPYC and simultaneous administration of PAH (10 μM). Scale bar, 100 μm. N = 3, **P < 0.01, ***P < 0.001, ****P < 0.0001.

2.7. PAH@DECM significantly reduces side effects while achieving better therapeutic effects

In the aforementioned study, oral administration of PAH demonstrated favorable therapeutic effects on OA. However, we observed significant side effects in various organs of the rats. After oral administration of PAH, there was an increase in inflammatory cells in the lung tissue; the liver exhibited a loss of hepatic tissue; the spleen showed unclear boundaries between the red and white pulp, with the disappearance of splenic cords; the kidneys had increased inflammatory cell proliferation and damage to the renal corpuscles; no significant abnormalities were observed in the heart (Fig. 7A). For this purpose, we successfully prepared cartilage DECM hydrogel, which self-crosslinks into a gel at 37 °C. Following the addition of varying concentrations of PAH, the gelation time of the cartilage DECM hydrogel at 37 °C was significantly reduced, taking only 20 and 14 min, respectively (Fig. 7B). Scanning electron microscope (SEM) images (Fig. 7C) reveal the reticular porous structure of the cartilage DECM hydrogel. Compared to the unmodified form, the PAH@DECM hydrogel becomes increasingly dense and regular with escalating PAH concentrations, preserving its distinct reticular porous structure. The pore size of the PAH@DECM hydrogel ranges from 100 to 200 μm, which is beneficial for cell proliferation and the transfer of nutrients. Combining the hydrogel degradation ratio (Fig. 7D) and the PAH release percentage of the hydrogel (Fig. 7E), we found that PAH is gradually released as the hydrogel degrades. Notably, the incorporation of PAH significantly retards the degradation rate of the cartilage DECM hydrogel, thereby maintaining a therapeutic concentration of PAH within the joint. Next, we calculated the porosity of the hydrogel using the solution replacement method and found that the porosity of the hydrogel decreases as the PAH drug loading concentration increases (Fig. 7F). The above results indicate that loading with PAH alters the cross-linking degree of the cartilage DECM. The swelling behavior of the hydrogel indicates that the water absorption capacity of the cartilage DECM without PAH loading is 256 % of its own weight, while after loading with PAH, the swelling rate of PAH@-DECM increased to 357 % and 396 %, respectively, depending on the PAH concentration (Fig. 7G). This increase is predominantly attributable to the two hydroxyl groups present in PAH's molecular structure, which confer substantial hydrophilicity, thus enhancing the scaffold's swelling rate. Mechanical strength is an important parameter for evaluating the potential application of hydrogels in cartilage tissue engineering. The DECM hydrogel itself has relatively weak mechanical strength, but when used as a drug carrier, its ultimate strength gradually increases with the increase of PAH concentration, from 53 kPa to 122 kPa (Fig. 7H). In response to this phenomenon, we hypothesize that the simple DECM has a loose structure and a reticular form, leading to relatively low ultimate strength. However, during the loading process of PAH, the aldehyde groups of PAH chemically react with the amine groups of Col2 in the DECM, and the hydroxyl groups of PAH form hydrogen bonds with the hyaluronic acid in the matrix, ultimately enhancing the mechanical properties. The FTIR analysis of the DECM hydrogel revealed alterations in the peaks at 1041 cm^{-1} and 2359 cm^{-1}. The wavenumber region around 1041 cm^{-1} is typically indicative of the stretching vibrations associated with the C–O single bonds, suggesting that the phenolic hydroxyl groups of PAH may interact with the peptide chains, proteins, or polysaccharides within the DECM through hydrogen bonding, leading to the formation of a stable complex. The emergence of a new peak at 2359 cm^{-1} is likely related to the involvement of PAH in the polymerization reaction of the DECM, resulting in the creation of a novel polymeric network. These changes in the absorption peaks and the associated bonding interactions indicate that the incorporation of PAH is actively involved in the crosslinking process of the DECM (Fig. 7I). In prior research, it was noted that PAH enhanced chondrocyte proliferation (Fig. 3G). To further investigate whether PAH, when integrated with DECM to form PAH@DECM, maintains its ability to stimulate cell proliferation, we conducted an additional CCK-8 assay. The results showed no significant difference in cell proliferation among the three groups on the first day of chondrocyte culture (Fig. 7J). However, differences emerged after the third day, with PAH-loaded DECM demonstrating stronger proliferation-promoting capabilities. By the seventh day of culture, the proliferation-promoting ability of the PAH@DECM hydrogel group was significantly higher than that of the DECM group, with higher concentrations of PAH showing better effects. Immunofluorescence staining (Fig. 7K) and cell migration experiments (Fig. 7L) revealed that compared to the DECM group, chondrocytes grew and spread well in the PAH@DECM hydrogel. With increasing PAH loading concentrations, there was improved cell proliferation and migration, consistent with the CCK8 results. To verify that the PAH@DECM hydrogel does not affect the efficacy of PAH, we conducted animal experiments using the previously mentioned DMM rat model.The results showed that compared to oral administration of PAH, the PAH@DECM hydrogel demonstrated a better therapeutic effect on OA, with reduced cartilage loss in rats. Relying on the biocompatibility of DECM with the ECM within the joint cavity, the targeting action of PAH was further enhanced. Immunohistochemical results showed that the PAH@DECM hydrogel exhibited a stronger ability to suppress the expression levels of EPYC and IL-17A (Fig. 7M). The above results demonstrate that the PAH@DECM hydrogel we constructed has advantages in sustained release, targeting, swelling, and mechanical strength, which can minimize side effects and achieve better therapeutic effects in OA.

3. Methods

3.1. Retrieval from GEO database

To establish an OA diagnostic model, The mRNA expression profile data for GSE55235 and GSE55457 were obtained from the GEO database (https://www.ncbi.nlm.nih.gov/geo/), following the methodologies outlined in the referenced literature [36,37]. GSE55235 includes sequencing data of cartilage samples from 10 OA patients and 10 normal controls. GSE55457 includes sequencing data of cartilage samples from 10 OA patients and 10 normal controls.

3.2. Construction of osteoarthritis Rat model

All surgical procedures adhered strictly to the guidelines set by the National Institutes of Health (NIH) for the care and use of laboratory animals. These procedures received approval from the Animal Ethics Committee of Shanghai Tenth People's Hospital, affiliated with Tongji University School of Medicine, under the approval number SHDSYY-2023-3825. Male SD rats (age: 8 weeks; weight: 300–320 g) were purchased from Shanghai Jiesjie Experimental Animal Co. (Approval Number: SCXK 2023–0004, Shanghai, China), and an OA knee joint rat model was established by surgically damaging the medial meniscus (DMM). In brief, the rats were randomly divided into three groups, named the Sham group, DMM group and the PAH group. Prior to the sham surgery, rats in the Sham group were anesthetized intraperitoneally with 35 mg/kg pentobarbital. The skin and joint capsule were incised, followed by sequential suturing of the joint capsule and skin. In the OA group, the medial meniscus and anterior cruciate ligament were excised, and the joint capsule and skin were sutured. Postoperatively, each rat was injected with ibuprofen to alleviate pain and given penicillin to prevent infection. Three days after surgery, the rats were forced to exercise on a custom treadmill for 1 h daily for six weeks. In the PAH group of rats, PAH was administered orally at a dose of 8 mg/kg/day every other day for a continuous period of 14 days following the DMM treatment.

3.3. Histological slice preparation

Rats were euthanized by an overdose injection of 8 % pentobarbital (40 mg/kg). The knee joints were excised and fixed in 4 % (v/v)

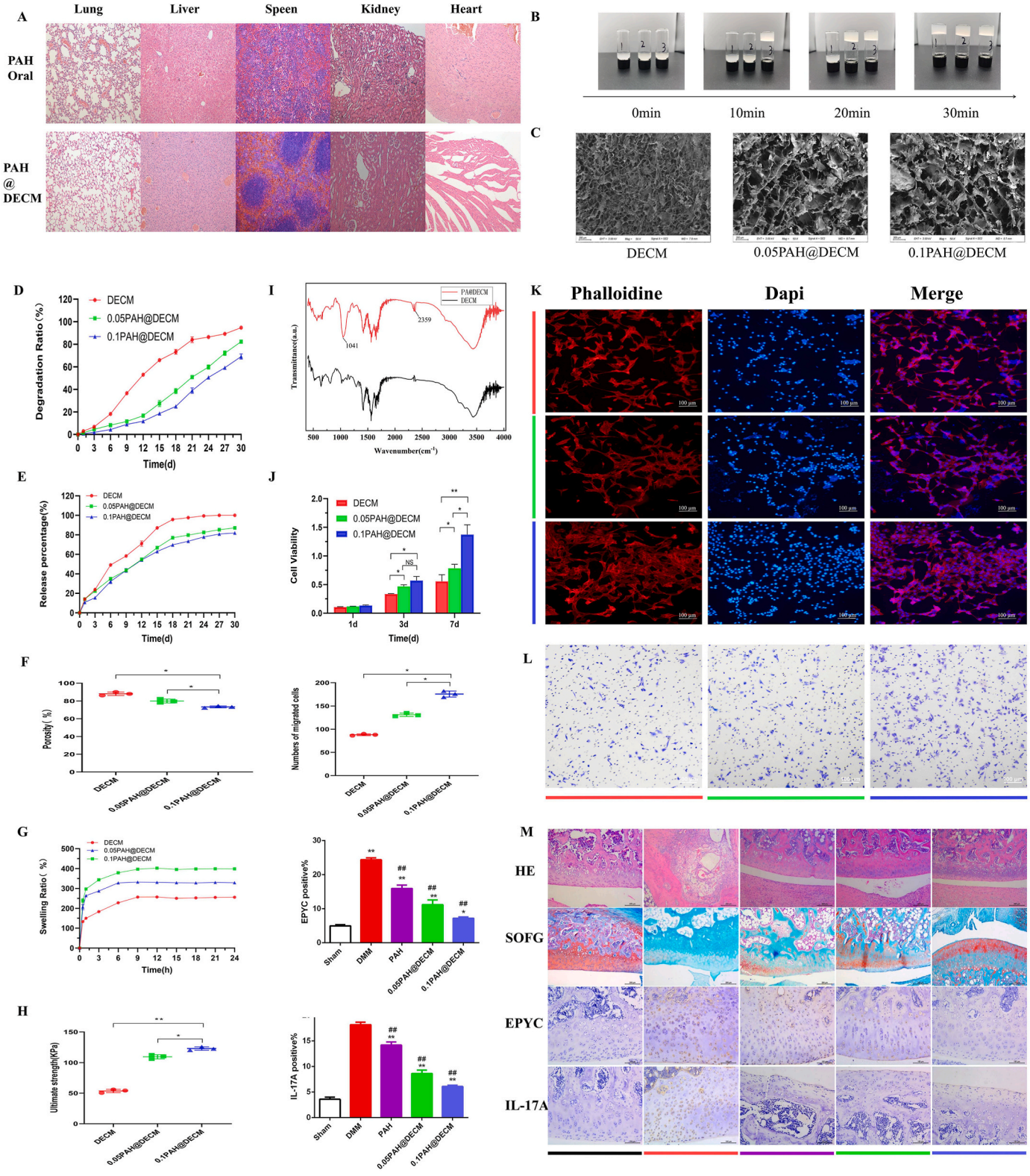

(caption on next page)

Fig. 7. Characterization of PAH@DECM Hydrogel Materials. (A) After oral administration of PAH and intra-articular injection of PAH@DECM, side effects were observed in rat organ sections through HEstaining. (B) Illustration depicting the alteration in gelation time following the addition of PAH. 1: DECM group; 2: 0.05PAH@DECM group; 3: 0.1PAH@DECM group. (C) SEM images of scaffold morphologies for three groups. Scale bar, 200 μm. EHT = 3.00 kV Mag = 50X Siganl A = SE2 (D) Degradation rates of various scaffold systems over time. N = 3. (E) Drug release rates of PAH over time in the three scaffold systems. N = 3. (F) Porosity measurements of the three different scaffold systems. N = 3, *P < 0.05. (G) Swelling rates over time for the three scaffold systems. N = 3. (H) The ultimate strength of the three scaffold systems. N = 3, *P < 0.05, **P < 0.01. (I) The FTIR analysis of the dECM hydrogel revealed alterations in the peaks at 1041 cm^{-1} and 2359 cm^{-1}. (J) Results from the CCK8 assay observing the effects of the three scaffold systems on chondrocyte proliferation at three time points: 1 day, 7 days, and 14 days. (K) Conducting immunofluorescence experiments, Actin staining was utilized to observe the spread and growth of chondrocytes across the three scaffold systems, while Dapi staining was employed to assess the impact of each scaffold system on chondrocyte proliferation. Scale bar, 100 μm, N = 3. (L) Transwell experiments were conducted to observe the changes in cell migration capabilities of chondrocytes after growth on the three different scaffold systems. Scale bar, 100 μm, N = 3, *P < 0.05. (M) Observation on pathological sections from DMM rat models to compare the therapeutic effect of PAH@DECM intra-articular injection on OA and its regulatory impact on EPYC and IL-17A, in contrast to the simple intra-articular injection of PAH. Scale bar for H&E and SOFG, 200 μm, Scale bar for EPYC and IL-17A, 100 μm. N = 3, *P < 0.05, **P < 0.01, compared with Sham group. #P < 0.05, compared with DMM group.

paraformaldehyde (PFA) for 24 h. Subsequently, the joints were decalcified in 10 % (v/v) ethylenediaminetetraacetic acid (EDTA) for 4 weeks, with fresh EDTA replacement every 2 days. For subsequent staining analysis, specimens were dehydrated, embedded in paraffin, and sliced into 0.5 μm thick slides in the sagittal plane.

3.4. H&E staining and SOFG staining

Rats were raised for 6 weeks, after which they were euthanized, and their knee joints were harvested. The knee joints were then fixed in 10 % formaldehyde at 4 °C for a period exceeding 48 h. Subsequently, a decalcification process was conducted in a 0.5 mol/L EDTA solution with a pH of 7.4 for a duration of 14 days. Following decalcification, the specimens were embedded in paraffin. The paraffin blocks were subsequently sectioned into 5 μm slices, and staining was performed according to standardized procedures utilizing H&E staining reagents (Servicebio, G1005-1) and SOFG staining reagents (Solarbio, G2540 G1371). Evaluation was carried out using the scoring system established by the OARSI [38].

3.5. EdU cell proliferation assay and quantification

Chondrocytes were seeded in culture dishes and allowed to adhere overnight. For proliferation assessment, cells were incubated with 10 μM EdU (Beyotime, C0071S) for 4 h. Post-incubation, cells were fixed with 4 % paraformaldehyde for 15 min at room temperature and permeabilized with 0.5 % Triton X-100 for 20 min. The EdU incorporation was detected using a Click-iT EdU Alexa Fluor 488 Imaging Kit, following the manufacturer's instructions. This involved applying the Click-iT reaction cocktail to the cells, allowing the reaction to proceed for 30 min protected from light. After washing with 3 % BSA in PBS, cell nuclei were counterstained with DAPI for 5 min.

3.6. Western Blots

Following RIPA lysis, protein lysate samples were obtained from each group. The protein concentration within the samples was determined using the BCA technique. Protein samples were separated by SDS-polyacrylamide gel electrophoresis (SDS-PAGE) and subsequently transferred to a polyvinylidene fluoride (PVDF) membrane. The PVDF membrane was blocked in 5 % BSA solution at room temperature for 2 h and then incubated overnight at 4 °C with the primary antibody. After washing with TBST solution, the secondary antibody was incubated at room temperature for 1 h. Subsequently, the membrane was washed three times with TBST solution and protein bands were visualized using ECL reagent and the Tanon 5200 chemiluminescence imaging system. Gray values were assessed using Image J software. The primary antibodies used in this experiment included anti-EPYC antibody (Novusbio, 70,338), anti-β-actin antibody (Service, GB11001), anti-IL-17A antibody (Affinity, DF6227)

3.7. Gene expression analyze

Total RNA was extracted and purified from processed cells using TRIzol Reagent (Invitrogen). RNA concentration was determined using a Multiskan Go (Thermo Scientific) instrument. Samples were then reverse transcribed from RNA to cDNA using the PrimeScript RT Master Mix Kit (TAKARA). Real-time PCR analysis was performed using SYBR Premix Ex *Taq*II (TAKARA) following the manufacturer's instructions. Glyceraldehyde-3-phosphate dehydrogenase (GAPDH) was used as an internal reference control. The sequences involved in this study are as follows.

Genes	Sequence 5' -3'
Rat actin beta-RT-F	CACCCGCGAGTACAACCTTC
Rat actin beta-RT-R	CCCATACCCACCATCACACC
Rat Col2a1 –F	TGTATGGAAGCCCTCGTCCT
Rat Col2a1 –R	TGCCCCTTTGGCCCTAATTT
Rat Aggrecan –F	TCGGATCCCCAAATCCCTCA
Rat Aggrecan –R	GTAGCTCGGAAGGCATAAGCA
Rat MMP-13 –F	ACCATCCTGTGACTCTTGCG
Rat MMP-13 –R	TTCACCCACATCAGGCACTC
Rat ADAMTS5 –F	AGTACAGTTTGCCTACCGCC
Rat ADAMTS5 –R	AGGACACCTGCGTATTTGGG
Rat EPYC –F	ATGTGCCACCAAGACAAATGA
Rat EPYC –R	GTTGGTGCAGCCAATGTAGC
Rat IL-17A –F	TGAAGGCAGCGGTACTCATC
Rat IL-17A –R	GGGTGAAGTGGAACGGTTGA

3.8. Enzyme-linked Immunosorbent assay

Chondral tissues from each group of rats were processed with pre-chilled physiological saline in a specified ratio. The chondral tissues were homogenized into 10 % tissue homogenate using a 1 mL homogenizer and centrifuged at 10,000 rpm for 10 min. Subsequently, the supernatant was collected and distributed. The supernatant obtained from the chondral tissues was analyzed using an IL-17A ELISA kit (Elabscience, E-EL-M0047). The detailed steps were performed following the instructions provided with the kit.

3.9. Immunohistochemical staining

Tissue sections were prepared for immunohistochemical staining. Antigen retrieval was performed by incubating the sections with 0.1 % trypsin at 37 °C for 40 min or by incubating with citrate buffer at 95 °C for 20 min. The following primary antibodies were used for immunohistochemistry: EPYC antibody (Novusbio, 70,338) and IL-17A antibody (Affinity, DF6227).

3.10. Immunofluorescent staining

Tissue sections were prepared for immunofluorescence staining. After dewaxing the sections in xylene and ethanol, antigen retrieval was performed at 37 °C in a 2 mg/mL trypsin solution for 1 h. Subsequently,

the sections were immersed in PBS three times for 5 min each, followed by blocking with 10 % goat serum at room temperature for 2 h and incubation with various primary antibodies at 4 °C for 8 h. The sections were then washed three times with PBST solution and incubated in the dark at room temperature with the corresponding secondary antibodies for 1 h. After staining the cell nuclei with DAPI, the sections were observed and photographed under a fluorescence microscope (Olympus, Japan). The primary antibodies used in the experiment included anti-IL-17A antibody (Affinity, DF6227) and anti-IL-17RA antibody (Abcam, Ab180904).

3.11. Procurement and cultivation of chondrocytes and synoviocyte

Chondrocytes were obtained from Wuhan Procell (CP-R092), and synoviocytes were procured from Wuhan Procell (CP-R083). Both chondrocytes and synoviocytes were cultured in DMEM medium supplemented with 10 % fetal bovine serum and 1 % penicillin-streptomycin-glutamine. Cell growth was maintained in a humidified incubator at 37 °C with 5 % CO2.

3.12. Construction of a synoviocyte-chondrocyte Co-culture model

The experimental procedure involved the pre-treatment of rat chondrocytes with IL-1β (10 ng/m) for a duration of 24 h. These pre-treated chondrocytes were then resuspended at a concentration of 1 × 10^5 cells per well, with a total volume of 2 mL. Subsequently, they were introduced into the lower chambers, specifically designed as 6-well migration chambers (SARSTEDT, 83.3930.041). The upper chambers were prepared by seeding rat synoviocytes at a density of 1 × 10^5 cells per well within 6-well plates. The culture medium utilized was DMEM, generously supplemented with 10 % FBS. Incubation conditions were maintained at 37 °C with 5 % CO2 in a humidified incubator. Following an incubation period spanning 24–48 h, the lower cell population was harvested for subsequent analyses.

3.13. Molecular docking experiments

To conduct a detailed analysis of the binding affinities and interaction mechanisms between PAH and EPYC, we utilized AutodockVina 1.2.2, an advanced in silico protein–ligand docking software. The molecular structure of PAH was meticulously sourced from the PubChem Compound database (https://pubchem.ncbi.nlm.nih.gov/). Concurrently, the 3D coordinates of EPYC were precisely acquired from the Protein Data Bank (PDB) (http://www.rcsb.org/pdb/home/home.do). In our docking analysis, all protein and molecular files underwent a rigorous conversion to PDBQT format, ensuring the exclusion of all water molecules and the addition of polar hydrogen atoms for enhanced accuracy. The grid box was strategically centered to encompass the domain of each protein while allowing for unimpeded molecular movement. This grid box was configured to dimensions of 30 Å × 30 Å × 30 Å, with a grid point distance meticulously set at 0.05 nm. The molecular docking studies were conducted with precision using Autodock Vina 1.2.2 (http://autodock.scripps.edu/), ensuring a comprehensive and accurate representation of the molecular interactions under investigation.

3.14. Co-immunoprecipitation

Primary chondrocytes were cultured in DMEM with supplements, stimulated with IL-17A, and then lysed using RIPA buffer. The cell lysates underwent pre-clearance with protein A/G agarose beads to reduce non-specific binding. This was followed by overnight incubation with anti-IL-17A antibody (Cell signal , 13838s), after which protein A/G agarose beads were added to the mixture for complex formation. Subsequent to washing the beads to remove unbound proteins, the protein complexes were eluted and subjected to SDS-PAGE and Western blot analysis. Immunoblotting was performed using an anti-IL-17RA antibody (Abcam , Ab180904) and visualized using an ECL system. The binding affinity between IL-17A and IL-17RA was quantified using image J, ensuring the use of appropriate controls for validation. It is critical to maintain cold conditions throughout the process and to select specific antibodies for accurate results.

3.15. Cytotoxicity analyzes

Cell proliferation was measured using the Cell Counting Kit-8 (CCK-8, Biosharp, BS350B) as per the manufacturer's instructions. Chondrocytes were initially cultured under optimal conditions until an adequate level of confluence was achieved. This stage was followed by the administration of IL-17A at a concentration of 50 ng/mL to the cultured cells. Subsequently, these cells were subjected to a series of treatments with PAH at various concentrations, namely 0, 1 μM, 2 μM, 5 μM, and 10 μM. Post-PAH exposure, the cells were incubated with the CCK-8 solution, allowing sufficient time for colorimetric development. Absorbance readings were then meticulously acquired using a spectrophotometer at the 450 nm wavelength; 50 μL of hydrogel was spread on a 96-well plate. After gelation, chondrocytes were seeded on the hydrogel and incubated in proliferation medium. After 3 and 7 days of co-cultivation, 100 μL of CCK-8 solution was added and incubated in a 5 % CO2 incubator at 37 °C for 2 h. The absorbance was measured at 450 nm using a spectrophotometer. The cells were then fixed, permeabilized, and incubated with actin working solution at room temperature for 2 h, followed by the addition of DAPI to observe cell growth on the hydrogel scaffold. Cell counting was performed, and the data were represented as the mean ± SD of three replicates.

3.16. Preparation of PAH@DECM hydrogel

We utilized the DECM preparation method developed by Freytes [39], briefly summarized as follows: Porcine knee joints were purchased from a local market, from which the cartilage was stripped, washed with PBS, treated with liquid nitrogen, pulverized, and then incubated in 1 % TritonX-100 solution at room temperature for 48 h. The decellularized matrix pieces were then removed, thoroughly rinsed with PBS, lyophilized, ground into powder, and stored. Subsequently, the dry decellularized matrix and pepsin were dissolved in 0.01 mol/L HCl, agitated at 37 °C for 24 h, followed by the addition of PAH to prepare the drug solutions with concentrations of 0.05 mol/L and 0.1 mol/L, designated as PAH@DECM pre-gels (0.05PAH@DECM and 0.1PAH@DECM). The pH was adjusted to 7.4 on ice to form a cold pre-gel, which was then stored at 4 °C. This was subsequently placed at 37 °C to observe gel formation.

3.17. SEM observation

Using a scanning electron microscope (SEM) to observe the network-like porous structure of PAH@DECM. Different groups of hydrogels were immersed in 2 mL of PBS at 37 °C for 24 h to reach swelling equilibrium. After freeze-drying the hydrogels, they were cut into small pieces longitudinally and then gold-coated for direct observation using a scanning electron microscope, the thickness of the metal film deposited is approximately 5–10 nm.

3.18. Porosity analysis

We calculated the porosity of the hydrogel using the solvent replacement method. In brief, a Petri dish was filled with anhydrous ethanol at room temperature and weighed, denoted as m1. A hydrogel with a mass of ms was immersed in anhydrous ethanol for 1 h, and the entire assembly was weighed as m2. After removing the sample, the remaining assembly was weighed as m3. The porosity of the hydrogel was calculated using the following formula: Porosity (100 %) = [(m2 -

m3 - ms)/(m1 - m3)] × 100 %.

3.19. Analysis of PAH release and In vitro degradation analysis of the scaffold

We measured the absorbance at 280 nm using a UV–Vis spectrophotometer and calculated the release amount by comparing it to a standard concentration. In summary, the hydrogel was soaked in PBS in a 24-well plate, and every 3 days within a 30-day period, 100 μl of the solution was taken and replenished with 100 μl of fresh PBS. The released PAH was quantified, and the release rate was used to quantitatively analyze the release capability of PAH in PAH@DECM. The hydrogel was placed in a PBS lysozyme solution (containing 10 μg/mL lysozyme, pH = 7.4), and cultured at 37 °C. Every 3 days during a 30-day period, the supernatant was removed, washed twice with deionized water, dried, and weighed. The weight was denoted as mt, and the weight on the 0th day was m0. The degradation rate D (100 %) was calculated using the formula: D (100 %) = (m0 - mt)/m0 × 100 %. Data are presented as the mean ± SD of three replicates.

3.20. Swelling analysis

Cylinder-shaped cross-linked samples were immersed in PBS at 37 °C for different durations: 1 min, 3 min, 5 min, 10 min, 30 min, 1 h, 1.5 h, 2 h, 2.5 h, 3 h, and 4 h. After each specified time interval, the samples were removed and weighed, denoted as mt. Finally, they were freeze-dried, and the dry weight was recorded as md. The swelling ratio (100 %) was calculated using the following formula: S = [(mt - md)/md] × 100 %.

3.21. Mechanical Property testing

The mechanical properties of the hydrogel were tested through compression experiments under a loading mode. Cylindrical hydrogel samples (5 mm in height, 10 mm in diameter, n = 4) were prepared and placed on the lower platen at a speed of 1 mm/min. The compression force was continuously recorded until the hydrogel deformed under the upper platen.

3.22. Cell migration assay

To investigate the effect of PAH@DECM on chondrocyte migration, 1 × 10^5 chondrocytes in serum-free medium were seeded in the upper chamber of a Transwell system (BD Falcon, USA), with different hydrogels added to the lower chamber. Migration was allowed for 8 h. Cells in the upper chamber were then removed, and the remaining cells on the lower surface of the Transwell were fixed with 4 % paraformaldehyde. After staining with 0.2 % crystal violet, migrated cells were visible under a microscope.

3.23. Fourier transform infrared spectroscopy

The chemical structure and the integrity of chemical bonds within the scaffold are assessed using Fourier transformed infrared spectroscopy (FTIR), with spectral analysis conducted over a wavenumber range of 500–4000 cm^{-1}。

3.24. Statistical analysis

The experimental results presented in this study were analyzed using Prism 7.0 software (GraphPad Prism). Data are expressed as mean ± standard deviation (SD). Statistical significance between two or multiple groups was calculated using the two-tailed Student's t-test or two-way ANOVA, followed by Dunnett's test for multiple comparisons. A P-value of less than 0.05 was considered statistically significant.

3.25. Disscussion

OA is a chronic degenerative disease characterized by chronic inflammation and cartilage degeneration [40,41]. Under pathological conditions, the equilibrium between ECM degradation and synthesis in articular chondrocytes is disrupted, leading to chondrocyte apoptosis and the loss of joint cartilage. In this study, we found that the expression level of EPYC, a component of ECM, is significantly upregulated in OA, and its level is closely related to the progression of OA. Concurrently, PAH can exert its anti-inflammatory effects in OA, thereby serving a therapeutic role in OA. By constructing in vivo and in vitro models of EPYC overexpression and knockdown in OA, we discovered that the expression level of EPYC regulates the expression of IL-17A in the body and mediates the effects of IL-17A on chondrocyte hypertrophy and proliferation phenotypes. Mechanistically, EPYC promotes the binding of the inflammatory chemokine IL-17A, secreted by synovial cells, to the chondrocyte surface receptor IL-17RA. This interaction activates downstream signals of the IL-17 signaling pathway, leading to chondrocyte hypertrophy, inhibition of chondrocyte proliferation, and exacerbation of OA progression. PAH indirectly inhibits the activation of the IL-17 signaling pathway by modulating the expression level of EPYC, suppresses chondrocyte hypertrophy, and enhances chondrocyte proliferation, thereby exerting a therapeutic effect on OA. To our knowledge, this is the first study to validate the therapeutic effect of the natural phenolic compound PAH on OA. Furthermore, this paper is the first to report that EPYC promotes the progression of OA by regulating the binding of IL-17A to its receptor IL-17RA.

The data we obtained from the GEO database shows that compared to healthy individuals, patients with OA exhibit abnormal activation of leukocytes, dysregulation of chemokine activity, disruption of chemokine-mediated signaling pathways, and perturbation of chemokine homeostasis (Fig. 2B). Chemokines are closely associated with inflammation, which in turn has a complex relationship with changes in the inflammatory microenvironment. The KEGG results showed that most differentially expressed genes are associated with the IL-17 signaling pathway (Fig. 2C). The IL-17 signaling pathway has been repeatedly reported to be related to OA. IL-17 is a family of six cytokines (IL-17A-F), with IL-17A being the most studied and significant [17,31,32,42]. Studies have shown that the extracellular matrix (ECM) regulates the activation state of cells by blocking or facilitating the binding of cytokines to cell surface receptors.

The IL-17 signaling pathway has been reported to play a significant role in OA. Wang et al. have shown that the stimulation of chondrocytes with IL-17 triggers the production of reactive oxygen species, Monocyte Chemoattractant Protein-1 (MCP-1), and IL-1β. This is accompanied by an increase in aging-associated β-galactosidase activity, prolongation of the resting/gap phase (G0/G1) in the cell cycle, and a reduction in the duration of the S phase of DNA synthesis. Collectively, these effects result in premature senescence of chondrocytes and a worsening of osteoarthritis [32]. Another study has demonstrated that IL-17 treatment of chondrocytes activates the NF-κB and MAPK signaling cascades and upregulates the expression of metabolic factors involved in cartilage degradation, such as IL-6, MMP3, and A Disintegrin And Metalloproteinase with Thrombospondin Motifs 4 (ADAMTS-4). This promotes the breakdown of the cartilage matrix, disrupts the internal homeostasis of the cartilage, and intensifies the progression of OA [43]. Our experimental results demonstrate that EPYC significantly activates the IL-17 signaling pathway by promoting the binding of IL-17A to the chondrocyte surface receptor IL-17RA, thereby aggravating the progression of OA. Studies have confirmed that IL-17A can also exert effects through signaling pathways such as the NF-kb pathway, MAPK pathway, and MAP kinase pathway [44]. The synergistic interaction between IL-17 and TNF-α can activate the production of pro-inflammatory mediators such as IL-1β, IL-6, IL-8, PGE2, and MMPs, thus facilitating the progression from early inflammation to chronic arthritis [45]. The research findings regarding the IL-17 signaling pathway are consistent

with the results of this study.

Cartilage tissue is predominantly composed of the ECM, which accounts for over 90 % of its total volume, with chondrocytes making up less than 10 %. The ECM's collagen and PGs are the primary macromolecules that endow articular cartilage with its load-bearing capabilities. In the early phases of OA, there is often a disruption in the metabolism of proteoglycans. The ECM is pivotal in the pathology of OA, with its degradation being a significant indicator of the disease's onset. Chondrocytes, the sole organized cells within articular cartilage, are responsible for synthesizing the dense components of the ECM. They are instrumental in maintaining cartilage homeostasis by balancing the metabolism of ECM degradation and synthesis. The cartilage's ECM is essential for preserving its biomechanical properties, enabling it to distribute pressure and shear stress during joint motion and to provide resilient support.EPYC is a component of ECM that interacts with collagen fibers and proteoglycan, promoting the formation of type I collagen fibers [12] and playing a significant role in cartilage development and the maintenance of joint integrity [13]. Recently, EPYC has been reported to potentially play an important role in OA [14], but the underlying mechanisms remain to be elucidated. Our study comprehensively validates the regulatory role of EPYC in chondrocyte hypertrophy and proliferation.

The natural phenolic compound PAH is reported to have anti-inflammatory effects. PAH is known to reduce the secretion of pro-inflammatory cytokines, such as TNF-α and IL-6, by inhibiting the MAPK pathway, thus playing a role in the treatment of septic shock [46]. Additionally, it has been proven to protect human dermal fibroblasts from photoaging by inhibiting the expression of matrix metalloproteinases and pro-inflammatory factors [25]. We discovered that PAH also exerts an anti-inflammatory role in OA, mediating its pharmacological effects through its modulation of EPYC. Overall, our research emphasizes the key role of EPYC in regulating chondrocyte hypertrophy and proliferation. EPYC enhances the binding of the inflammatory chemokine IL-17A to its chondrocyte surface receptor IL-17RA, thereby further activating the IL-17 signaling pathway and exacerbating the trend of OA. Conversely, PAH inhibits the expression of EPYC, indirectly suppressing the IL-17 signaling pathway, and preventing the further exacerbation of OA. The research findings regarding the PAH are consistent with the results of this study.

In addition to mechanistic studies, we have also provided a practical approach for clinical translation of PAH delivery, by combining DECM with PAH for intra-articular injection. DECM is a biological material crafted by eliminating cellular components from biological tissues while retaining the ECM's three-dimensional architecture and bioactive molecules. Owing to its hydrogel characteristics and excellent biocompatibility, DECM is increasingly becoming a focal point in tissue engineering research. The process of creating DECM hydrogels involves techniques such as freeze-drying, grinding, enzymatic digestion, and neutralization with alkali to adjust the solution's ion concentration. These hydrogels, which coagulate at lower temperatures and take shape at 37 °C, demonstrate favorable biological attributes. However, the preparation of DECM hydrogels through modifications in pH, salt, ion concentration, and temperature can only achieve a certain level of gelation and does not significantly enhance the mechanical properties of the DECM hydrogel. Further advancements are necessary to improve the mechanical integrity of these biomaterials for effective tissue repair and regeneration, The solution we propose is that the crosslinking interaction between PAH and the DECM hydrogel prevents rapid decomposition and excessive swelling of the matrix. Furthermore, during the slow degradation of the DECM hydrogel, PAH is steadily released into the joint. This approach initially circumvents the first-pass effect of PAH and enhances the drug concentration within the arthritic cavity, thereby mitigating drug side effects. Furthermore, This demonstrates good drug-loading and controlled-release capabilities, swelling capacity, appropriate degradation, and porosity, thereby enhancing drug efficacy. Corresponding cell and animal experiments have shown that PAH@DECM can further enhance the therapeutic effects of PAH for OA, presenting a viable drug delivery material for the clinical application of PAH in OA treatment. However, our study also has some limitations. there are aspects of this study that warrant further refinement. Our research has conclusively demonstrated that EPYC plays a regulatory role in the progression of OA. Nonetheless, the upstream mechanisms responsible for the upregulation of EPYC expression throughout the disease course of OA are not yet fully understood. We aim to investigate these mechanisms in subsequent studies. This dedicated effort aims to establish a robust groundwork for its prospective utilization as an innovative biomarker in diagnosing OA, thereby charting a novel therapeutic trajectory for OA management.

4. Ethics approval and consent to participate

All surgical procedures adhered strictly to the guidelines set by the National Institutes of Health.

(NIH) for the care and use of laboratory animals. These procedures received approval from the.

Animal Ethics Committee of Shanghai Tenth People's Hospital, affiliated with Tongji University.

School of Medicine, under the approval number SHDSYY-2023-3825. Male SD rats (age: 8 weeks; weight: 300–320 g) were purchased from Shanghai Jiesjie Experimental Animal Co. (Approval Number: SCXK 2023–0004, Shanghai, China)

Consent for publication

All authors have reviewed and approved the final version of the manuscript for publication.

Funding

This work is supported by grants from Shanghai Municipal Science and Technology Commission Natural Science Fund (20ZR1443200 to Peng Wu, China), Shanghai Municipal Health Commission Clinical Research General Project Fund (03.02.22.007 to Peng Wu, China), Shanghai Tenth People's Hospital Research Physician Class A Fund (2023YJXYSA004 to Peng Wu, China), Shanghai Tenth People's Hospital National Natural ScienceFoundation Internal Incubation Project Fund (04.03.19.122 to Peng Wu, China), the Youth Program of Medical Engineering Cross Research Fund of Shanghai Jiaotong University (YG2021QN93 to Sudan Xu, China).

Conflict of interst

The authors declare no conflict of interest.

CRediT authorship contribution statement

Junchao Huang: Writing – review & editing, Writing – original draft, Project administration, Formal analysis, Data curation, Conceptualization. **Ziheng Bu:** Writing – review & editing, Writing – original draft, Project administration, Formal analysis, Data curation. **Wei Liu:** Writing – review & editing, Writing – original draft, Project administration, Formal analysis, Data curation, Conceptualization. **Zheng Zhou:** Project administration, Formal analysis, Data curation. **Jianhai Hu:** Project administration, Formal analysis, Data curation. **Jianing Yu:** Project administration, Formal analysis, Data curation. **Huajun Wang:** Supervision. **Sudan Xu:** Supervision, Funding acquisition. **Peng Wu:** Supervision, Funding acquisition.

Declaration of generative AI and AI-assisted technologies in the writing process

During the preparation of this work the authors used ChatGPT4 in

order to refine and enhance the language and clarity of the manuscript. After using this tool, the authors reviewed and edited the content as needed and takes full responsibility for the content of the publication.

Declaration of competing interest

The authors declare that they have no known competing financial interests or personal relationships that could have appeared to influence the work reported in this paper.

Data availability

Data will be made available on request.

Acknowledgements

We extend our heartfelt gratitude to the entire team at the Shanghai Tenth People's Hospital Affiliated Center for Orthopaedic Science and Translational Medicine for their invaluable assistance and support throughout this research project. Their commitment to excellence and willingness to share expertise significantly contributed to the success of our study. We also express our appreciation for the provision of state-of-the-art equipment and facilities, which were crucial in facilitating our research endeavors. The collaborative environment and the dedicated efforts of all members at the center have been instrumental in achieving the objectives of our study.

Appendix A. Supplementary data

Supplementary data to this article can be found online at https://doi.org/10.1016/j.mtbio.2024.101124.

References

[1] J.W. Bijlsma, F. Berenbaum, F.P. Lafeber, Osteoarthritis: an update with relevance for clinical practice, Lancet 377 (2011) 2115–2126.
[2] D.J. Hunter, D. Schofield, E. Callander, The individual and socioeconomic impact of osteoarthritis, Nat. Rev. Rheumatol. 10 (2014) 437–441.
[3] S.R. Goldring, M.B. Goldring, Changes in the osteochondral unit during osteoarthritis: structure, function and cartilage-bone crosstalk, Nat. Rev. Rheumatol. 12 (2016) 632–644.
[4] R.F. Loeser, S.R. Goldring, C.R. Scanzello, M.B. Goldring, Osteoarthritis: a disease of the joint as an organ, Arthritis Rheum. 64 (2012) 1697–1707.
[5] M.M. Sun, F. Beier, M.A. Pest, Recent developments in emerging therapeutic targets of osteoarthritis, Curr. Opin. Rheumatol. 29 (2017) 96–102.
[6] Y.T. Gu, J. Chen, Z.L. Meng, W.Y. Ge, Y.Y. Bian, S.W. Cheng, et al., Research progress on osteoarthritis treatment mechanisms, Biomed. Pharmacother. 93 (2017) 1246–1252.
[7] Y. Wu, Z. Hong, W. Xu, J. Chen, Q. Wang, J. Chen, et al., Circular RNA circPDE4D protects against osteoarthritis by binding to miR-103a-3p and regulating FGF18, Mol. Ther. 29 (2021) 308–323.
[8] R. Liu-Bryan, R. Terkeltaub, Emerging regulators of the inflammatory process in osteoarthritis, Nat. Rev. Rheumatol. 11 (2015) 35–44.
[9] Q. Wang, A.L. Rozelle, C.M. Lepus, C.R. Scanzello, J.J. Song, D.M. Larsen, et al., Identification of a central role for complement in osteoarthritis, Nat Med 17 (2011) 1674–1679.
[10] S. Yang, J. Kim, J.H. Ryu, H. Oh, C.H. Chun, B.J. Kim, et al., Hypoxia-inducible factor-2alpha is a catabolic regulator of osteoarthritic cartilage destruction, Nat Med 16 (2010) 687–693.
[11] Z. Yang, H. Li, J. Hao, H. Mei, M. Qiu, H. Wang, et al., EPYC functions as a novel prognostic biomarker for pancreatic cancer, Sci. Rep. 14 (2024) 719.
[12] Y. Tatara, I. Kakizaki, S. Suto, H. Ishioka, M. Negishi, M. Endo, Chondroitin sulfate cluster of epiphycan from salmon nasal cartilage defines binding specificity to collagens, Glycobiology 25 (2015) 557–569.
[13] S. Nuka, W. Zhou, S.P. Henry, C.M. Gendron, J.B. Schultz, T. Shinomura, et al., Phenotypic characterization of epiphycan-deficient and epiphycan/biglycan double-deficient mice, Osteoarthritis Cartilage 18 (2010) 88–96.
[14] Y. Liang, F. Lin, Y. Huang, Identification of biomarkers associated with diagnosis of osteoarthritis patients based on Bioinformatics and Machine learning, J Immunol Res 2022 (2022) 5600190.
[15] E. Lubberts, The IL-23-IL-17 axis in inflammatory arthritis, Nat. Rev. Rheumatol. 11 (2015) 562.
[16] N. Amatya, A.V. Garg, S.L. Gaffen, IL-17 signaling: the yin and the yang, Trends Immunol. 38 (2017) 310–322.
[17] J.Y. Mimpen, M.J. Baldwin, A.P. Cribbs, M. Philpott, A.J. Carr, S.G. Dakin, et al., Interleukin-17A causes osteoarthritis-like transcriptional changes in human osteoarthritis-derived chondrocytes and synovial fibroblasts in vitro, Front. Immunol. 12 (2021) 676173.
[18] Y. Liu, H. Peng, Z. Meng, M. Wei, Correlation of IL-17 level in synovia and severity of knee osteoarthritis, Med. Sci. Mon. Int. Med. J. Exp. Clin. Res. 21 (2015) 1732–1736.
[19] S. Glyn-Jones, A.J. Palmer, R. Agricola, A.J. Price, T.L. Vincent, H. Weinans, et al., Osteoarthritis. Lancet 386 (2015) 376–387.
[20] E. Krustev, D. Rioux, J.J. McDougall, Mechanisms and mediators that drive arthritis pain, Curr. Osteoporos. Rep. 13 (2015) 216–224.
[21] Z.Q. Chang, E. Gebru, S.P. Lee, M.H. Rhee, J.C. Kim, H. Cheng, et al., In vitro antioxidant and anti-inflammatory activities of protocatechualdehyde isolated from Phellinus gilvus, J. Nutr. Sci. Vitaminol. 57 (2011) 118–122.
[22] C.Y. Moon, C.R. Ku, Y.H. Cho, E.J. Lee, Protocatechuic aldehyde inhibits migration and proliferation of vascular smooth muscle cells and intravascular thrombosis, Biochem. Biophys. Res. Commun. 423 (2012) 116–121.
[23] G. Wei, Y. Guan, Y. Yin, J. Duan, D. Zhou, Y. Zhu, et al., Anti-inflammatory effect of protocatechuic aldehyde on myocardial ischemia/reperfusion injury in vivo and in vitro, Inflammation 36 (2013) 592–602.
[24] Y. Xu, W.L. Jiang, S.P. Zhang, H.B. Zhu, J. Hou, Protocatechuic aldehyde protects against experimental sepsis in vitro and in vivo, Basic Clin. Pharmacol. Toxicol. 110 (2012) 384–389.
[25] Y. Ding, C. Jiratchayamaethasakul, S.H. Lee, Protocatechuic aldehyde attenuates UVA-induced photoaging in human dermal fibroblast cells by suppressing MAPKs/AP-1 and NF-kappaB signaling pathways, Int. J. Mol. Sci. 21 (2020).
[26] A. Urciuolo, L. Urbani, S. Perin, P. Maghsoudlou, F. Scottoni, A. Gjinovci, et al., Decellularised skeletal muscles allow functional muscle regeneration by promoting host cell migration, Sci. Rep. 8 (2018) 8398.
[27] T.J. Keane, S.F. Badylak, The host response to allogeneic and xenogeneic biological scaffold materials, J Tissue Eng Regen Med 9 (2015) 504–511.
[28] E. Sanchez-Lopez, R. Coras, A. Torres, N.E. Lane, M. Guma, Synovial inflammation in osteoarthritis progression, Nat. Rev. Rheumatol. 18 (2022) 258–275.
[29] J. Huang, J. Lin, C. Li, B. Tang, H. Xiao, Palovarotene can attenuate heterotopic ossification induced by tendon stem cells by downregulating the synergistic effects of smad and NF-kappaB signaling pathway following stimulation of the inflammatory microenvironment, Stem Cell. Int. 2022 (2022) 1560943.
[30] J. Huang, J. Wu, J. Lin, C. Li, B. Tang, H. Xiao, Palovarotene inhibits the NF-kappaB signalling pathway to prevent heterotopic ossification, Clin. Exp. Pharmacol. Physiol. 49 (2022) 881–892.
[31] J. Xiao, P. Zhang, F.L. Cai, C.G. Luo, T. Pu, X.L. Pan, et al., IL-17 in osteoarthritis: a narrative review, Open Life Sci. 18 (2023) 20220747.
[32] H.J. Faust, H. Zhang, J. Han, M.T. Wolf, O.H. Jeon, K. Sadtler, et al., IL-17 and immunologically induced senescence regulate response to injury in osteoarthritis, J. Clin. Invest. 130 (2020) 5493–5507.
[33] A. Askari, M.M. Naghizadeh, R. Homayounfar, A. Shahi, M.H. Afsarian, A. Paknahad, et al., Increased serum levels of IL-17a and IL-23 are associated with decreased vitamin D3 and increased pain in osteoarthritis, PLoS One 11 (2016) e0164757.
[34] C. Deligne, S. Casulli, A. Pigenet, C. Bougault, L. Campillo-Gimenez, G. Nourissat, et al., Differential expression of interleukin-17 and interleukin-22 in inflamed and non-inflamed synovium from osteoarthritis patients, Osteoarthritis Cartilage 23 (2015) 1843–1852.
[35] X. Wang, R. Sun, X. Hao, Z.X. Lian, H. Wei, Z. Tian, IL-17 constrains natural killer cell activity by restraining IL-15-driven cell maturation via SOCS3, Proc. Natl. Acad. Sci. U. S. A. 116 (2019) 17409–17418.
[36] J. Huang, D. Liu, J. Zhang, H. Xiao, A network pharmacology study: reveal the mechanisms of palovarotene against heterotopic ossification, Front. Med. 9 (2022) 897392.
[37] J. Huang, J. Zhang, H. Xiao, Identification of epigenetic-dysregulated lncRNAs signature in osteosarcoma by multi-omics data analysis, Front. Med. 9 (2022) 892593.
[38] K.P. Pritzker, S. Gay, S.A. Jimenez, K. Ostergaard, J.P. Pelletier, P.A. Revell, et al., Osteoarthritis cartilage histopathology: grading and staging, Osteoarthritis Cartilage 14 (2006) 13–29.
[39] D.O. Freytes, J. Martin, S.S. Velankar, A.S. Lee, S.F. Badylak, Preparation and rheological characterization of a gel form of the porcine urinary bladder matrix, Biomaterials 29 (2008) 1630–1637.
[40] J. Li, M. Jiang, Z. Yu, C. Xiong, J. Pan, Z. Cai, et al., Artemisinin relieves osteoarthritis by activating mitochondrial autophagy through reducing TNFSF11 expression and inhibiting PI3K/AKT/mTOR signaling in cartilage, Cell. Mol. Biol. Lett. 27 (2022) 62.
[41] J. Li, M. Jiang, C. Xiong, J. Pan, S. Jia, Y. Zhang, et al., KLF4, negatively regulated by miR-7, suppresses osteoarthritis development via activating TGF-beta1 signaling, Int. Immunopharm. 102 (2022) 108416.
[42] E. Lubberts, The IL-23-IL-17 axis in inflammatory arthritis, Nat. Rev. Rheumatol. 11 (2015) 415–429.
[43] G. Hu, N. Zhang, J. Li, J. Wang, W. Wu, J. Li, et al., Tumor necrosis factor receptor associated factor 3 modulates cartilage degradation through suppression of interleukin 17 signaling, Am. J. Pathol. 190 (2020) 1701–1712.

[44] Z. Huang, L. Xie, Y. Xu, K. Zhao, X. Li, J. Zhong, et al., Essential oils from zingiber striolatum diels attenuate inflammatory response and oxidative stress through regulation of MAPK and NF-kappaB signaling pathways, Antioxidants 10 (2021).
[45] C. Schinocca, C. Rizzo, S. Fasano, G. Grasso, L. La Barbera, F. Ciccia, et al., Role of the IL-23/IL-17 pathway in rheumatic diseases: an overview, Front. Immunol. 12 (2021) 637829.
[46] S. Wu, Q. Wang, J. Wang, B. Duan, Q. Tang, Z. Sun, et al., Protocatechuic aldehyde from Salvia miltiorrhiza exhibits an anti-inflammatory effect through inhibiting MAPK signalling pathway, BMC Complement Med Ther 20 (2020) 347.